Biomolecular Detection Assays

by
Victoria Marie Hlavinka

A dissertation submitted to the William A. Brookshire Department of Chemical and Biomolecular Engineering,
Cullen College of Engineering
in partial fulfillment of the requirements for the degree of

DOCTOR OF PHILOSOPHY

in Chemical and Biomolecular Engineering

Chair of Committee: Richard C. Willson

Committee Member: Mehmet Orman

Committee Member: Katerina Kourentzi

Committee Member: Sergey Shevkoplyas

Committee Member: Chandra Mohan

University of Houston
May 2022

DEDICATION

This dissertation is dedicated to the educators whose devotion has been imperative to my personal and professional growth. I also dedicate this work to my parents, who were my first teachers.

ACKNOWLEDGEMENTS

I would like to extend my most sincere gratitude to my advisor, Dr. Richard Willson, for allowing me to work in his lab and contribute to the present work. I am fortunate to have an advisor who actively supports my research interests while still encouraging diligence for the task at hand. I also would like to thank Dr. Katerina Kourentzi, who provided much guidance throughout my entire PhD. I especially appreciate her help at the beginning of my graduate work when I was new to the lab and her willingness to serve on my committee. Dr. Binh Vu has played a significant role in the success of this project, for which I am incredibly grateful. Since I started working in the lab, Katerina and Binh have acted as my mentors and helped develop various techniques used in this work. Special thanks to Drs. Mehmet Orman, Sergey Shevkoplyas, and Chandra Mohan for their insight and service on my dissertation committee.

Several students in Dr. Willson's labs at the University of Houston and Tecnológico de Monterrey have contributed their knowledge, time, and skill to the development of this work. Thank you to Dr. Mary Crum, Dr. Gavin Garvey, Dr. Ujwal Patil, Dr. Max Smith, Dr. Heather Goux, Dr. Ahmad Nazem, Dr. Dimple Chavan, João Trabuco, Kristen Brosamer, Atul Goyal, Suman Nandy, Rongwei Lei, Vijay Maranholkar, and Anjali Drugkar for their helpful advice and friendship. Special thanks to Kristen for her LFA knowledge. At TdM, Dr. Federico Ruiz-Ruiz, Dr. Patricia Vazquez, Dr. Mirna González-González, Dr. Margarita Ortiz Martínez, and Calef Sánchez-Trasviña have done outstanding work, notably in the analysis of our diabetic saliva samples, led by Prof. Marco Rito-Palomares, their Associate Dean of Graduate Studies and Research. I am also grateful for our collaboration with the Clinicas del

Azúcar and Drs. Omar Meza Ledezma and Alexandro José Martagón Rosado in Monterrey and Mexico City, whose patients were recruited for this study.

Finally, I want to thank my family and friends for all their guidance and encouragement. I am grateful to my parents, Laura and Michael Hlavinka, my brother, sister-in-law, and niece, Alex, Elizabeth, and Margaret Hlavinka, and friends Matthew and Monica Carlin for being my greatest supporters.

ABSTRACT

In the present work, three methods for the detection or monitoring of biomolecules are outlined in detail. The first study describes the development of a saliva-based enzymatic screening assay for diabetes mellitus. In the second study, lateral flow assays (LFAs) utilizing commercial colloidal gold and blue latex nanoparticle reporters are compared to persistent luminescence nanoparticle (PLNP; "nanophosphor") LFAs to assess the sensitivity of nanophosphors as a reporter system. The final study demonstrates the utility of a nanophosphor-based LFA for detecting low concentrations of dengue virus (DENV) biomarker non-structural protein 1 (NS1).

1,5-Anhydroglucitol (AHG) is a naturally occurring monosaccharide and a clinically validated blood biomarker for diabetes. The blood concentration of AHG falls during periods of hyperglycemia, as glucose outcompetes AHG for kidney reuptake. Salivary AHG quantification has been suggested to be useful for diabetes screening but has not been implemented in any widely applicable fashion. We have developed a chemiluminescence assay to quantify AHG in saliva and demonstrated that the assay could distinguish between healthy and diabetic individuals ($N = 265$; $p < 0.0001$, ROC AUC = 0.82). These findings suggest that, with further validation, this approach may serve as the basis of a non-invasive tool for diabetes screening.

Commercially-available LFAs commonly use colloidal gold or blue latex nanoparticles reporter systems that lack sensitivity and are prone to human error when interpreted visually. We have developed nanophosphors that can detect low levels of antigen. In a comparison study, a nanophosphor-based human immunoglobulin G (IgG) LFA had a limit of detection of 0.625 ng/mL, an 81-fold and 58-fold increase in sensitivity over colloidal gold and blue latex nanoparticles, respectively.

Current DENV diagnostic methods are commonly unspecific and cannot detect early infection. We have developed an inexpensive, rapid LFA to detect DENV NS1, a known marker of early dengue infection. Using strontium aluminate nanophosphors as reporters, we achieved a limit of detection of 1 ng/mL DENV serotype 1 NS1 antigen. Our assay is comparable to a laboratory-based NS1 ELISA with a 1 ng/mL limit of detection.

TABLE OF CONTENTS

LIST OF TABLES

LIST OF FIGURES

1. INTRODUCTION

The present work discusses recent advancements made in the detection of various biomolecules. Chapter 1 describes the motivation for the work and provides an in-depth background of the techniques used in biomolecular detection methods. Additionally, a review of the relevant literature and previous work regarding the present study is given.

Chapter 2 presents a saliva-based assay to screen for diabetes mellitus. Chapter 3 compares the quantification of human antibodies by different lateral flow assay reporter formats. Chapter 4 describes a point-of-care lateral flow assay to quantify low levels of dengue virus non-structural protein 1. Concluding remarks and suggestions for future work to further validate the results of the following studies are made in Chapter 5.

1.1. Biomolecular detection methods

The present work relies on several different methods of biomolecular detection to determine the presence or absence of target molecules. These methods include spectrophotometry or colorimetry, fluorescence, photoluminescence, and chemiluminescence.

Spectrophotometry is a detection method derived from electromagnetic spectroscopy that involves the quantitative measurement of the reflection or transmission of a material as a function of wavelength[1]. Similarly, colorimetry is a branch of spectrophotometry specifically concerned with wavelengths within the visible light spectrum and human color perception. The main component of a spectrophotometer is the photometer, which measures the strength of electromagnetic radiation to quantify the intensity of a light beam at different wavelengths. The light measured is commonly

within the ultraviolet, visible, or infrared spectra. However, modern spectrophotometers can measure light intensity over large portions of the spectral range, including x-ray and microwave wavelengths. Historically, spectrophotometers used monochromators containing a diffraction grating to produce the analytical spectrum at single, individual wavelengths at a time. If a photomultiplier tube or photodiode is used, the grating can be scanned stepwise so that the detector can measure light at several different wavelengths over time.

In biochemistry and biotechnology, spectrophotometry is a commonly used technique in experiments involving DNA, RNA, and protein analyses[2]. Spectrophotometry can be used in conjunction with Beer-Lambert's Law to determine the relationship between absorbance, transmittance, and concentration[3]. One typical example is the use of ultraviolet-visible (UV-vis) absorbance to measure the concentration of DNA, RNA, or proteins in solution. Additionally, spectrophotometry is used in several well-established biomolecular assay techniques, including enzyme-linked immunosorbent assays (ELISAs) and Western blots. Similarly, colorimetry is the fundamental determination technique in commercial lateral flow assays (LFAs) using colloidal gold or blue latex nanoparticle-conjugated antibodies.

Fluorescence is the emission of light due to excitation by a light source or other electromagnetic radiation. This property makes fluorescence a form of luminescence (light emission that does not result from heat). Compounds that emit fluorescent light are referred to as fluorophores. Generally, fluorophores are excited by the absorbance of radiation at lower wavelengths than the light they emit, which therefore has lower photon energy.

Instruments that measure fluorescent intensity are called fluorometers. Like spectrophotometers, fluorometers consist of a source of light that passes through a monochromator or filter and then passes through a sample. Separately, a second beam of light passes through an attenuator and is automatically adjusted to match the fluorescent intensity of the sample. Light from the sample and the attenuated light beam are detected by separate transducers and converted to an electrical signal interpreted by a computer system. Modern fluorometers can detect fluorescent compounds at concentrations as low as one part per trillion[4], making fluorescence orders of magnitude more sensitive than other techniques, such as UV-vis absorbance.

Fluorescence has applications in various industries, such as forensics, lighting and signage (e.g., fluorescent lamps and road signs), and medical imaging. Biomolecular assay techniques that use fluorescence include Western, Southern, and Northern blotting, fluorescence polarization, and quantitative polymerase chain reaction (qPCR). Lesser-known fluorescent biomolecular techniques such as Förster resonance energy transfer (FRET) and fluorescence-activated cell sorting (FACS) have become more common within the last two decades[5,6]. Commercial LFAs utilizing fluorescent nanoparticles are also available[7].

Photoluminescence is another form of luminescence initiated by photoexcitation, in which photons excite electrons in an atom to a higher energy level. Specifically, this work involves the use of phosphorescent nanoparticles—with phosphorescence being a type of photoluminescence closely related to fluorescence. When exposed to short-wavelength radiation, a phosphorescent substance will glow, absorbing the light and reemitting it at a longer wavelength for an extended time after the source of radiation has

been removed. In this way, phosphorescence is unlike fluorescence, as fluorescent materials immediately reemit the radiation they absorb.

When the dysprosium- and europium-doped strontium aluminate powder used in this work is exposed to light, it undergoes a process called persistent luminescence, in which a high-energy photon is absorbed, and its energy becomes trapped in the crystal lattice of the material. The trapped energy is stored until released by a random thermal or vibrational energy fluctuation. This property allows the material to emit light persistently for an extended time. Everyday examples of persistent luminescence materials are glow-in-the-dark toys and stickers, paint, and clock dials. Recently, developments have been made in the field of point-of-care diagnostics, where persistent luminescence nanophosphors of strontium aluminate have been used as reporter particles in LFAs[8,9].

Chemiluminescence is the emission of light due to a chemical reaction[10]. Benefits of chemiluminescent detection methods include ultra-sensitive detection limits, rapid detection of the chemiluminescent substrate, and its broad range of analytical applications. Clinical laboratories routinely use chemiluminescence for immunoassays in the form of a chemiluminescent label or as a chemiluminescent detection reaction for an enzyme label[11]. Other commonly used techniques such as Western, Northern, and Southern blotting also use chemiluminescence to measure enzymes expressed by reporter genes, cellular luminescence, blotted proteins, and nucleic acids[12].

Historically, luminol was the first compound used as a chemiluminescent label[13]. When in the presence of horseradish peroxidase, luminol in the presence of a suitable oxidant, such as hydrogen peroxide, undergoes peroxidase-catalyzed oxidation[14]. The light emission intensity from this reaction is proportional to the peroxidase activity.

Several other chemiluminescent technologies exist, such as acridinium ester and sulfonamide labels used in chemiluminescent immunoassays that produce a flash of light when exposed to an alkaline hydrogen peroxide solution[15]. For a screening assay for diabetes mellitus, we use a lesser-known chemiluminescent reagent for the direct detection of hydrogen peroxide, Lumigen HyPerBlu, that does not require any peroxidase[16]. The light produced by this chemistry is colloquially named "glow" luminescence, as the intensity increases gradually over a long period rather than in a short burst of light, as is the case with chemiluminescent detection techniques using acridinium ester and sulfonamide labels. The rate at which the intensity increases depends on the concentration of the light-producing substrate—hydrogen peroxide. Therefore, solutions with a high peroxide concentration will produce light faster than those with low concentrations, resulting in an overall greater luminescent intensity. Additionally, HyPerBlu is highly sensitive and unaffected by many quenching compounds or inhibition of coupling enzymes, unlike chemiluminescent detection using horseradish peroxidase labels. HyPerBlu avoids these interferences by utilizing a technology based on a specific reaction to produce luminescence de novo.

1.2. Diabetes mellitus and its current diagnostic methods

Diabetes mellitus, commonly referred to as diabetes, is a severe, chronic disease where the body's endocrine system cannot regulate blood glucose concentration. This defect leads to an abnormally high amount of circulating glucose, or hyperglycemia, which may eventually cause lasting damage to other major organ systems. It is estimated that over 420 million adults live with some form of diabetes, and it is suspected that millions more unknowingly have the disease[17]. Diabetes can be challenging to recognize

in its early stages, as symptoms tend to be unspecific and develop slowly. Common initial symptoms of diabetes include increased urination, thirst, hunger, and unintentional weight loss.

There are several different forms of diabetes, but two types are most prevalent: type 1 and type 2 diabetes. Although all classes result in unregulated blood glucose concentration, the etiology of the disease differs among the types of diabetes. Type 1 diabetes, formerly known as Insulin-Dependent Diabetes Mellitus, is chronic hyperglycemia due to an insulin deficiency[17]. This type of diabetes is thought to result from the immune-mediated destruction of pancreatic β cells that produce insulin[18,19]. Though it can be diagnosed at any age, type 1 diabetes is one of the most common chronic childhood diseases, with peak presentation between ages 5-7 years and at or near puberty[20–22]. Management of this form of the disease often includes insulin analogs delivered via injection and other technologies such as insulin pumps and continuous glucose monitors[23].

In contrast, type 2 diabetes develops due to insulin resistance associated with obesity, little physical activity, and poor diet. In addition to resistance, there may be reduced insulin secretion in patients with type 2 diabetes[17]. Although typically diagnosed in adults and the elderly, the disease has recently been observed in children and adolescents with increasing incidence[24]. Except in severe cases, the first form of intervention for insulin-resistant diabetes is adopting a healthy lifestyle to manage the disease and prevent or delay the onset of complications[25]. Nevertheless, due to the progressive nature of type 2 diabetes, lifestyle changes are generally not adequate to maintain glycemic control over time, meaning that patients will eventually have to

include some form of medication in their treatment. Several classes of anti-diabetic drugs are currently available for this purpose, primarily aimed at increasing pancreatic insulin production, increasing the sensitivity of the insulin receptor, or reducing the rate at which glucose is absorbed by the digestive tract[26]. Unfortunately, these medications have been demonstrated to cause increased mortality and heart failure, in conjunction with other harmful side-effects[26].

Having diabetes also drastically increases the risk of developing long-term complications, especially in those with diabetes who have not been diagnosed and are not receiving treatment. Severe complications often include irreversible blood vessel damage and vascular diseases such as cardiovascular disease, stroke, and peripheral artery disease[27]. Blood vessel damage may also affect the eyes, a condition known as diabetic retinopathy; this condition is the leading cause of vision loss in adults aged 20-74 years[28,29]. Diabetic nephropathy, or “diabetic kidney," may also develop due to vascular damage, possibly requiring dialysis or kidney transplantation[30]. However, the most common complication due to diabetes is diabetic neuropathy, which is nerve damage directly due to hyperglycemia and decreased blood flow to nerves as a result of vascular damage[17]. Nearly half of all patients with diabetes will have some form of nerve damage, and up to 24% experience “significant neuropathic pain[31].” Diabetic neuropathy often results in diabetic foot disease, where ulceration of the feet due to changes in nerves and vasculature requires subsequent limb amputation. It can be one of the most expensive complications of diabetes, especially in areas without access to adequate footwear[17].

Due to the significant burden imposed by diabetes, early diagnosis of the disease is pertinent for the prognosis of the patient and the health of society and the global

economy. Since 1980, the number of people with diabetes has nearly quadrupled from 108 million to 422 million in 2014, making the disease prevalence over 8% of adults worldwide, and is expected to be higher at present[32]. Additionally, diabetes contributed to over 3.5 million deaths in 2012 alone.[17] In total, the direct annual cost of diabetes to the world due to emergency and inpatient hospital care, medications, medical supplies, and long-term care is more than 827 billion US dollars[33,34]. In 2004, the World Health Organization and the International Diabetes Federation formed the "Diabetes Action Now" program to combat the global prevalence of diabetes by raising awareness of the disease and its complications[35]. Two of the five core functions of the program relate directly to developing and standardizing the surveillance and diagnosis of diabetes, emphasizing the importance of early detection of the disease[36].

Establishing a diagnosis and assigning the type of diabetes for an individual patient can be challenging and often depends on the circumstances at the time of diagnosis. Not all patients clearly fit within a single type, and clinical presentation may vary significantly[37]. Diabetes is commonly diagnosed from multiple criteria to verify the diagnosis and determine the type. Generally, diagnostic methods are based on circulating glucose concentration or the amount of glycated hemoglobin A_{1c} (HbA1c) in the blood[38]. HbA1c is a stable hemoglobin variant formed *in vivo* by the covalent attachment of glucose to the hemoglobin amino acids and was previously shown to have a clinical relationship to plasma glucose concentration[39,40]. The recommended target HbA1c concentration for adults is less than 6.5%, or 48 mmol/mol if it can be achieved without hypoglycemia (Table 1.1)[41]. HbA1c is a clinically useful index of mean glycemia for the preceding two to three months, the average lifespan of red blood cells[42]. From the HbA1c

concentration, the average blood glucose concentration, or estimated average glucose (eAG), can be determined; HbA1c concentrations higher than 6.5% may indicate a hyperglycemic event within the previous 120 days[43]. However, while HbA1c levels are not affected significantly by small fluctuations in blood glucose concentration, such as after a meal, they are reportedly influenced by race, age, and conditions that shorten red blood cell survival, such as sickle cell anemia and HIV[44]. Additionally, this method of diagnosis may not be comfortable for the patient, as it requires him or her to give a blood sample for analysis.

Total glucose concentration in plasma has traditionally been the most reliable and commonly used method for diabetes diagnosis[45]. This measurement is determined by either a fasting plasma glucose (FPG) assay or an oral glucose tolerance test (OGTT)[38]. The objective of an FPG assay is to evaluate the amount of glucose in plasma normally circulating in the body. A patient is considered diabetic when his or her FPG is greater than 7 mmol/L, or 126 mg/dL, or prediabetic between 110 and 126 mg/dL (Table 1.1)[44,46]. In contrast, an OGTT examines the endocrine system's response to a large influx of glucose. By determining the plasma glucose concentration before and two hours after consuming a 75 g glucose beverage, physicians can observe the patient's glucose tolerance[37]. A healthy individual should have a plasma glucose concentration of less than 11 mmol/L, or 200 mg/dL (Table 1.1)[44]. Though FPG and OGTT are the preferred methods to detect diabetes, these assays can be inconvenient and require strict patient adherence to the protocol, which is challenging to schedule and verify in a screening context.

Table 1.1. Criteria for the diagnosis of diabetes

Healthy	Prediabetes	Diabetes
HbA1c < 5.7%	5.7% ≤ HbA1c < 6.5%	HbA1c ≥ 6.5%
FPG < 110 mg/dL	110 mg/dL ≤ FPG < 126	FPG ≥ 126 mg/dL
OGTT < 140 mg/dL	140 mg/dL ≤ OGTT < 200 mg/dL	OGTT ≥ 200 mg/dL

Table 1.2 Major risk factors for type 2 diabetes

Family history of diabetes (i.e., parents or siblings with diabetes)
Overweight (BMI ≥ 25 kg/m^2)
Habitual physical inactivity
Race/ethnicity (e.g., African Americans, Hispanic Americans, Native Americans, Asian Americans, and Pacific Islanders)
Previously identified as prediabetic
Hypertension (≥ 140/90 mmHg in adults)
HDL cholesterol ≤ 35 mg/dL (0.90 mmol/L) and/or a triglyceride level ≥ 250 mg/dL (2.82 mmol/L)
Delivery of a baby weighing > 9 lbs
Polycystic ovary syndrome

The American Diabetes Association recommends that screening of the general population for type 2 diabetes should be completed by their health care provider every three years beginning at age 45 years[38]. However, screening should be considered at a younger age or completed more frequently in individuals presenting with two or more of the risk factors in Table 1.2.[38]

In low-resource settings where access to adequate healthcare is limited, point-of-care devices, such as glucose meters, can be used to screen for diabetes if laboratory

services are not available[47]. Moreover, due to the lack of medical facilities in these areas, the Global Action Plan for the Prevention and Control of Non-Communicable Diseases was established by the World Health Organization to improve accessibility to affordable testing and treatment for diseases such as diabetes to reduce their morbidity[48].

1.3. Lateral flow assays

Lateral flow assays (LFAs) are point-of-care or -need tests used to detect an analyte efficiently and economically, without specialized equipment or personnel for operation. Because of their simplicity, LFAs have become widely used in the medical, food, and agricultural industries. Operating on the same basic affinity chromatography principles as the enzyme-linked immunosorbent assay (ELISA), LFAs can detect biomolecules as a competitive or sandwich immunoassay. Unlike ELISAs, an LFA primarily consists of pads based on a series of capillary beds, such as nitrocellulose or silica-based porous membranes, on which capture or reporter conjugated-antibodies are immobilized[49]. For a sandwich LFA, as the liquid sample flows through the capillaries of the porous membranes, the target analyte present in the sample binds to the reporter-antibody conjugate at the conjugate release pad. Subsequently, the antigen binds to the capture antibody present at the test line. Similarly, any remaining unbound reporter-antibody conjugates are captured by antibodies specific to the conjugated antibody at the control line.

The most widely available commercial LFA is the home pregnancy test, which commonly uses either colloidal gold or colored (blue) latex nanoparticles as its reporters[49]. As the reporter-conjugated antibody accumulates at either the test or control line of the LFA, a visible red or blue line will appear from the gold or blue latex

nanoparticles, respectively, with lines appearing at both the test and control lines signifying a positive result or a single line at the control denoting a negative result.

Instrument-based reporters such as up-converting phosphors, magnetic microparticles, and fluorescent labels support more sensitive LFAs. However, these assays often require costly laboratory equipment, defeating the purpose of a point-of-care test. We have developed strontium aluminate persistent luminescent nanoparticles (PLNPs; "nanophosphors") as LFA reporters[9]. Upon excitation, the europium- and dysprosium-doped strontium aluminate nanophosphors ($SrAl_2O_4$: Eu^{2+}, Dy^{3+}) emit a long-lasting, bright glow that allows for a delayed emission measurement, reducing background auto-fluorescence and eliminating the need for precision optical filters. Strontium aluminate nanophosphor LFAs reportedly have a minimum 10-fold higher sensitivity over colloidal gold LFAs[9]. Additionally, this reporter system allows for smartphone imaging and analysis, limiting the occurrence of false positives or negatives due to human error[8].

Like colorimetric reporters, such as gold or blue latex, reporter-antibody conjugates will bind at the test (via the antigen) or control line to produce a positive or negative result. However, because nanophosphors are photoluminescent, the LFA is analyzed by briefly exposing the strip to a light source, then imaging in complete darkness. Luminescence observed at the test and control lines determine the target antigen's presence (Fig. 1.1).

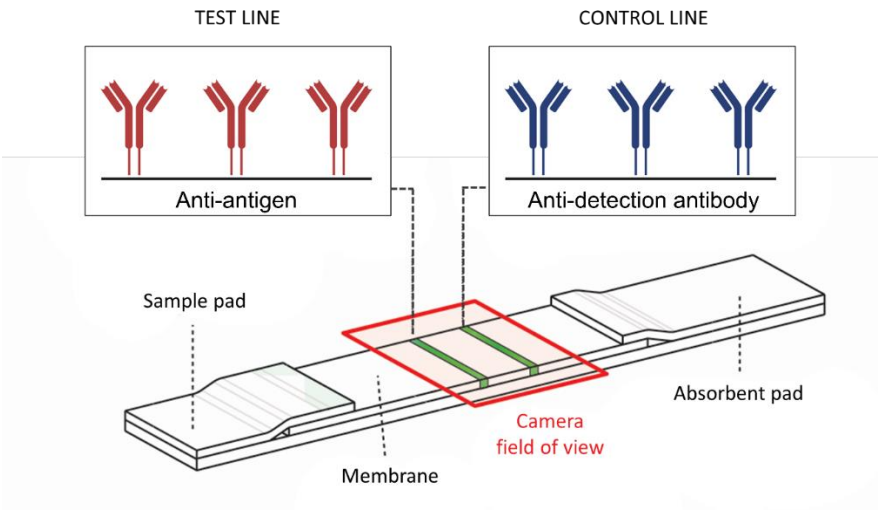

Figure 1.1. Schematic of a lateral flow assay.

1.4. Applications of IgG detection

Immunoglobulin G (IgG) is the most commonly found antibody in humans, representing approximately 75% of all serum antibodies[50]. A vital component of the immune response, IgG protects the body from infection by binding to foreign—or in the case of autoimmune disorders, innate—proteins present in tissues and blood. IgG antibodies participate predominantly in the secondary immune response[50]. When memory B cells recognize an antigen at its receptor, they release IgG antibodies specific to that antigen that will bind via their antigen-binding fragments (F_{ab})[51]. In addition to its F_{ab} site, IgG also contains a crystallizable fragment (F_c) which binds to the F_c receptor of cells to initiate phagocytosis[52].

Because of its participation in the immune response, IgG detection is a particularly useful tool in diagnosing various diseases, such as *Helicobacter pylori* infection, HIV, dengue virus, and SARS-CoV-2[53–56]. However, IgG quantification is also helpful in a variety of other unique applications, including monitoring monoclonal

antibody production and manufacturing[57]. Human immunoglobulin has been proposed as a specific marker for human fecal-water contamination, suggesting that human IgG potentially serves as a single-molecule marker for rapid, one-step detection of human fecal contamination in water sources[58].

1.5. Dengue virus and its current diagnostic methods

Dengue virus (DENV), a single-stranded RNA virus responsible for the disease known as dengue fever, infects an estimated 390 million people per year[59,60]. A mosquito (*Aedes aegypti*)-borne disease, dengue fever, is classified as a neglected tropical disease as it is endemic in the developing regions of Asia and South America[61]. Symptoms of dengue fever tend to be nonspecific and typically begin three to fourteen days following infection[62]. Common symptoms include high fever, headache, vomiting, muscle and joint pains, and a characteristic skin rash[60,62]. Some cases develop into a more severe condition, dengue hemorrhagic fever, resulting in bleeding, low levels of blood platelets, and blood plasma leakage that requires hospitalization[60,62].

There are four recognized serotypes of DENV and a possible fifth serotype that has yet to be fully validated[63,64]. All serotypes can cause dengue fever. Through a process known as antibody-dependent enhancement, individuals previously infected with DENV are more likely to develop severe disease when re-infected by a different serotype. This severity of re-infection is due to the existing DENV antibodies from the previous infection interfering with the immune response to the current serotype, leading to a higher viral load[65]. For this reason, the currently available vaccine is only recommended to seropositive individuals—people who have been previously infected with DENV[66].

The most common and least specific method for dengue diagnosis is clinical evaluation[67]. An individual may be diagnosed with dengue fever when he or she presents with fever and two or more of the following: headache, retro-orbital pain, myalgia, arthralgia, rash, hemorrhagic manifestations (including a positive tourniquet test), or leukopenia[68]. However, these are common symptoms of a wide variety of tropical diseases, such as Zika, chikungunya, malaria, leptospirosis, typhoid, and yellow fever.

Laboratory methods for diagnosing dengue fever include antibody serology, nucleic acid testing, and non-structural protein 1 (NS1) antigen detection. Antibody serology assays test for the presence of specific IgM or IgG antibodies in human serum. IgM and IgG ELISAs are the second most commonly used diagnostic tool after clinical evaluation[69]. However, IgM antibodies specific to a single DENV serotype are not detectable until four days after the onset of symptoms, reducing their usefulness in the clinical management of the disease[70]. Secondary cases, which tend to be more severe, reportedly show lower IgM concentrations that are undetectable in more than 20% of cases[71]. IgG antibodies, which do not appear until much later after symptom onset, are not a suitable biomarker for early DENV detection. Reverse transcriptase-polymerase chain reaction (RT-PCR) can detect DENV RNA with high sensitivity and specificity in a relatively short amount of time. However, there are significant barriers to using RT-PCR as a dengue diagnostic test. Notably, RT-PCR is viable for only a short time in the early stages of DENV infection when the virus is detectable[72,73].

NS1 is a glycoprotein excreted from DENV-infected cells of all serotypes that can be used as a marker to diagnose dengue infection[69,72]. Because of its presence in the acute phase of infection and specificity for DENV, NS1 is a valuable biomarker for early

dengue infection and a natural target for a rapid diagnostic test. Many commercial ELISAs for NS1 are currently available[73]. DENV NS1 lateral flow assays using colloidal gold nanoparticles as the reporter system are also available but lack the sensitivity to detect low levels of DENV NS1[74].

2. DIABETES MELLITUS SCREENING BY CHEMILUMINESCENT ENZYMATIC DETECTION OF 1,5-ANHYDROGLUCITOL IN SALIVA

2.1. Introduction

Diabetes mellitus is a chronic disease in which the endocrine system cannot regulate blood glucose concentration; the resulting episodes of hyperglycemia can cause lasting damage to major organ systems. It is estimated that over 460 million adults worldwide have diabetes, with up to 50% of affected unaware that they have the condition[75]. The United States prevalence of diabetes in adults is 13.3%, with 31 million Americans diagnosed as diabetic[75]. Early detection can be challenging, as symptoms tend to be unspecific and develop slowly.

Screening for diabetes most commonly relies upon measuring glycated hemoglobin A1c (HbA1c) in the blood or, less commonly, glucose in the blood or urine[38,44]. HbA1c is a clinically useful indicator of mean glycemia for the two to three months preceding testing[42]. However, while HbA1c is not affected significantly by transient fluctuations in blood glucose concentration, such as after a meal, it can be influenced by race, age, and conditions that shorten red blood cell survival, including sickle-cell anemia and HIV[44]. Blood sampling may be unpleasant for subjects, especially when screening a broad population for an undiagnosed disease with initially non-specific symptoms. While glucose concentration in plasma[45], either as fasting plasma glucose or in an oral glucose tolerance test[38], is a standard method of diabetes detection, these assays can be inconvenient and require strict patient adherence to protocols, which are difficult to schedule and verify in a screening context.

1,5-Anhydroglucitol (AHG; 1-deoxyglucose), a naturally occurring six-carbon monosaccharide similar in structure to glucose, is found in nearly all foods and is absorbed in the gut. Although present in human serum, AHG is not excreted at high concentrations in urine because it is normally reabsorbed by the kidneys[76] and maintained at relatively constant blood concentrations of 5.9-33.8 μg/mL. Under hyperglycemia, increased amounts of AHG are excreted in the urine because glucose competes with AHG for reabsorption by the glomeruli[77]. As a result, the concentration of AHG in the blood falls rapidly and remains low for approximately two weeks following an episode of hyperglycemia[78].

AHG was first suggested as a blood marker of glycemic control nearly four decades ago. In 1981, Akanuma et al. reported that AHG concentration is much lower in the plasma of diabetics compared to healthy individuals[79]. AHG concentration in plasma initially was measured using gas-liquid chromatography. A more convenient enzymatic colorimetric assay of blood AHG has been developed and extensively used in Japan since 1991 under the name GlycoMark®[80–82]. The assay was also FDA-cleared for monitoring glycemic control in the United States in 2003[83]. The GlycoMark assay quantitates AHG in serum or plasma at concentrations from 0.49 to 110 μg/mL, with healthy individuals normally between 10.2 – 33.8 μg/mL for males and 5.9 – 31.8 μg/mL for females (Table 2.1)[84]. The assay relies on the oxidation of AHG to 1,5-anhydrofructose and hydrogen peroxide by pyranose oxidase, an enzyme with broad substrate specificity which also acts on glucose and galactose (Figs. 2.1a, b, & c)[85]. The hydrogen peroxide produced by the reaction, nominally equimolar to the AHG in the sample, is quantified using horseradish peroxidase (HRP) and the chromogenic substrate N-ethyl-N-(2-hydroxy-3-sulfopropyl)-

3-toluidine. Because pyranose oxidase catalyzes the oxidation of all pyranoses with the liberation of peroxide, glucose must be first removed or converted into a species nonreactive with pyranose oxidase. The GlycoMark assay uses glucokinase and an ATP regeneration system to convert glucose to nonreactive glucose 6-phosphate (Fig. 2.1d)[83].

Table 2.1. 1,5-Anhydroglucitol reference intervals partitioned by gender and age with glycated hemoglobin and glucose values presented for comparison

	All tested	Males		Females	
		18-39 years	All males	18-39 years	All females
Mean AHG (μg/mL)	20.1	23.9	22.5	18.4	17.7
AHG 2.5th - 97.5th reference interval (μg/mL)			10.2 - 33.8		5.9 - 31.8
HbA1c (%)	5.3	5.3	5.3	5.2	5.3
Glucose (mmol/L)	4.8	4.8	4.9	4.6	4.7

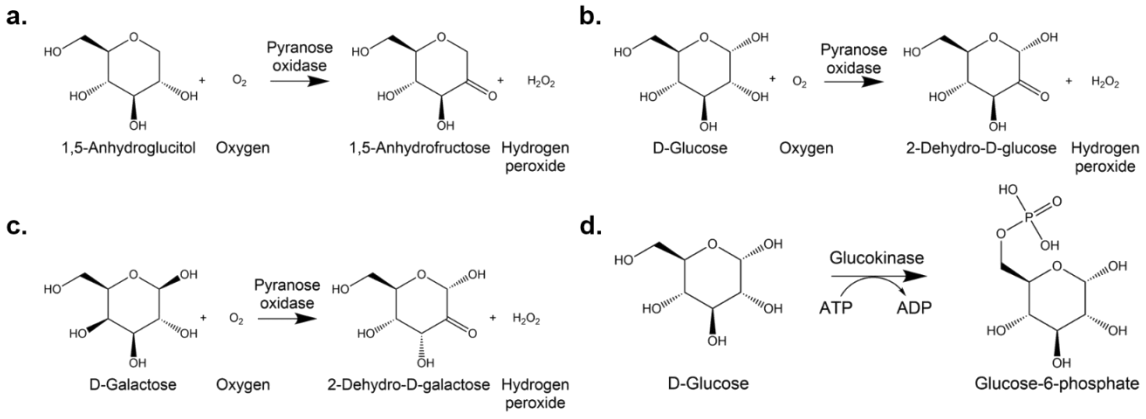

Figure 2.1. Oxidation of (a) 1,5-anhydroglucitol, (b) D-glucose, and (c) D-galactose catalyzed by pyranose oxidase. (d) Enzymatic conversion of D-glucose to glucose-6-phosphate by glucokinase.

Saliva is a clinically informative biological fluid of growing interest as a non-invasive diagnostic sample[86]. An unbiased search for non-invasive metabolic markers of diabetes by liquid chromatography and gas chromatography separation coupled with tandem mass spectrometry demonstrated a linear correlation between AHG concentrations in plasma and saliva[87]. Moreover, a strong negative association of AHG in saliva with diabetes was identified, suggesting that "[AHG] in saliva can be used in national screening programs for undiagnosed diabetes"[87]. An attempt was made to measure AHG in saliva using the GlycoMark assay. However, the results showed no correlation with saliva AHG concentrations determined by LC-MS and defined molecules that interfere with the GlycoMark assay[88].

Here we adapt the GlycoMark chemistry for use with saliva. We found that the prior difficulty was due to interfering substances in saliva absent from blood (e.g., galactose) and compounds that interfere with the GlycoMark assay chemistry, such as antioxidants. Salivary AHG also is too dilute for quantification by chromogenic reactions, requiring the development of a chemiluminescence assay.

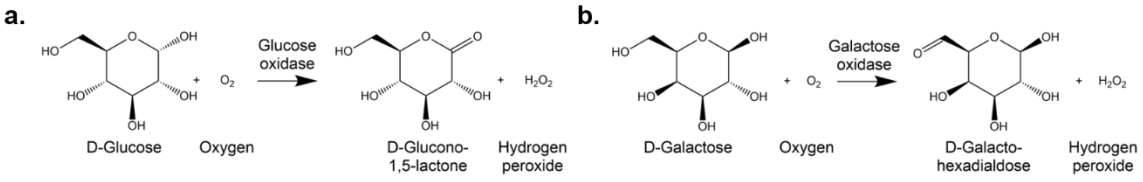

Figure 2.2. (a) Oxidation of D-glucose catalyzed by glucose oxidase. (b) Oxidation of D-galactose catalyzed by galactose oxidase.

We overcame these difficulties by enzymatically depleting glucose and galactose from saliva with glucose oxidase and galactose oxidase, respectively (Fig. 2.2). The

hydrogen peroxide produced is reduced by catalase, and ultrafiltration removes the pre-treatment enzymes from the sample. Finally, pyranose oxidase acts on AHG to produce hydrogen peroxide, which is sensitively detected by chemiluminescence. We identified a dioxetane-boronic acid chemiluminescent reagent whose emission is not quenched by antioxidants (e.g., uric acid) present in saliva, which quenches the luminol used in our first attempts (Figs. A.1-3). We optimized assay conditions and used it to test 265 saliva samples of nominally healthy and controlled diabetic individuals. We compared the results obtained from both groups as an initial assessment of the utility of this approach to identify diabetic individuals.

2.2. Methods

2.2.1. Materials

Glucose oxidase at 168.1 kU/g (1 U is equivalent to 1 μmol of product produced per minute) from Aspergillus niger, galactose oxidase at 1500 U/mg from Dactylium dendroides, pyranose oxidase at 10.4 U/mg from Coriolus sp., and catalase at 4998 U/mg from bovine liver were purchased from Sigma-Aldrich (St. Louis, MO). 1,5-Anhydroglucitol (AHG) 50 μg/mL calibration standard was purchased from GlycoMark (New York, NY). HyPerBlu chemiluminescent reagent was purchased from Lumigen (Southfield, MI). Sarstedt Salivette® cotton swabs were purchased from Thermo Fisher Scientific (Hampton, NH). Amicon Ultra 0.5 mL 3 kDa centrifugal filters were purchased from EMD Millipore (Burlington, MA).

2.2.2. Human subjects protocol

The sample collection protocol for this study was approved by the Institutional Review Board at the University of Houston (IRB ID CR00000501). Diabetic patients were recruited for this study from the Clínicas del Azúcar in Monterrey, Mexico (protocol approved by the Research Ethics Committee and Research Committee of the Tecnologico de Monterrey School of Medicine April 4, 2016). Written informed consent was obtained from all participants. All methods were performed in accordance with the relevant guidelines and regulations. Per the approved protocol, saliva samples were obtained from 210 adult patients who had been diagnosed as diabetic and were actively being treated with diet, exercise, medication, or a combination of these. The average HbA1c for diabetic patients was 7.39% (Std Dev 1.27%; range 5.37% - 10.04%). Additionally, 55 control samples were obtained from healthy adults without major systemic disorders.

2.2.3. Sample collection and preparation

Participants were asked to abstain from food or drink for 30 minutes before collection. For samples collected via Salivette, the participant placed the swab in his or her mouth and chewed it for two minutes to stimulate salivation, following Salivette protocol. Afterward, the swab was returned to the Salivette container and centrifuged at 3,500 g for two minutes. The filtrate was aliquoted and stored at -80°C. For samples collected by the passive drool method, the participant was asked to pool saliva in the front of his or her mouth, then transfer the saliva into a clean 15 mL tube until 3 mL of liquid was collected. Following collection, the passive drool saliva specimens were centrifuged, and the supernatant was aliquoted and stored at -80°C.

2.2.4. Preliminary comparison of control and diabetic saliva

Thawed saliva was treated with 0.2 U glucose oxidase (100 U/mL in PBS, pH 7.4), 1 U galactose oxidase (500 U/mL in PBS, pH 7.4), and 4 U catalase (2000 U/mL in PBS, pH 7.4) per 100 µL sample. The samples were incubated overnight at 37°C to ensure that glucose and galactose were fully depleted from the saliva. After incubation, the saliva was ultrafiltered using 3 kDa Amicon centrifugal filters by centrifuging at 14,000 g for 30 minutes to remove the enzymes, and 50 µL of the filtrate was added to individual wells of a white 96-well, half-area well plate. To begin the oxidation of AHG to hydrogen peroxide, 5.4 mU of pyranose oxidase (2.7 U/mL in PBS, pH 7.4) was added to each well, and 50 µL of HyPerBlu reagent was added to initiate light production from the hydrogen peroxide. The kinetic luminescence was immediately measured under the conditions described in the "Kinetic luminescent intensity recording" section below. The overall luminescent intensity of the samples at 700 seconds was used to evaluate the relative concentration of AHG in the saliva.

2.2.5. Interferent depletion optimization

2.2.5.1. Glucose depletion

To thawed saliva, 3 µL of catalase (5000 U/mL in PBS, pH 7.4) and 3 µL of glucose oxidase at 30, 300, or 3000 U/mL in 50 mM sodium acetate (pH 5) were added per 100 µL of saliva. The samples were then incubated at 37°C for 2, 10, 30, 60, or 120 minutes. Following incubation, the samples were transferred to an Amicon ultra 3 kDa centrifugal filter and centrifuged at 14,000 g for 30 minutes to remove the enzymes. 50 µL of the filtrates were pipetted into a white, half area 96-well plate, and 3 µL of glucose oxidase (3000 U/mL in 50 mM sodium acetate, pH 5) and 50 µL of room temperature

HyPerBlu were added to each well to detect any remaining glucose in the saliva samples. The kinetic luminescence was immediately measured as described in "Kinetic luminescent intensity recording" below. The rate of produced luminescence was determined for each tested clearance condition following the method described in "Data analysis."

2.2.5.2. Galactose depletion

To 100 µL of thawed saliva, 3 µL of catalase (5000 U/mL in PBS, pH 7.4) and 3 µL of galactose oxidase at 15, 150, or 1500 U/mL in 100 mM potassium phosphate (pH 6.0) were added. The samples were then incubated at 37°C for 2, 10, 30, 60, or 120 minutes. Following incubation, the samples were transferred to an Amicon ultra 3 kDa centrifugal filter and centrifuged at 14,000 g for 30 minutes to remove the enzymes. The filtrates (50 µL) were pipetted into a white, half area 96-well plate, and 3 µL of galactose oxidase (1500 U/mL in 100 mM potassium phosphate, pH 6.0) and 50 µL of room temperature HyPerBlu were added to each well to detect any remaining galactose in the saliva samples. The kinetic luminescence was immediately measured as described under "Kinetic luminescent intensity recording." The rate of produced luminescence was determined for each clearance condition as described under "Data analysis."

2.2.5.3. 1,5-Anhydroglucitol depletion

To thawed saliva, 3 µL each of catalase (5000 U/mL in PBS, pH 7.4), glucose oxidase (3000 U/mL in 50 mM sodium acetate pH 5.0), and galactose oxidase (1500 U/mL in 100 mM potassium phosphate, pH 6.0) and 3 µL of pyranose oxidase at 10, 100, or 1000 U/mL in 100 mM potassium phosphate (pH 7.0) were added per 100 µL of

saliva. The samples were then incubated at 37°C for 2, 10, 30, 60, or 120 minutes. Following incubation, the samples were transferred to an Amicon ultra 3 kDa centrifugal filter and centrifuged at 14,000 g for 30 minutes to remove the enzymes. The filtrates (50 µL) were pipetted into a white, half area 96-well plate, and 3 µL of pyranose oxidase (10 U/mL in 100 mM potassium phosphate, pH 7.0) and 50 µL of room temperature HyPerBlu were added to each well to detect any remaining glucose, galactose, and AHG in the saliva samples. The kinetic luminescence was immediately measured under the conditions described in the "Kinetic luminescent intensity recording" section. The rate of produced luminescence was determined for each clearance condition as described under "Data analysis."

2.2.6. 1,5-Anhydroglucitol quantification assay

2.2.6.1. Enzymatic clearance of saliva

Frozen saliva samples were thawed at room temperature, and 9 U glucose oxidase (3000 U/mL in 50 mM sodium acetate, pH 5), 4.5 U galactose oxidase (1500 U/mL in 100 mM potassium phosphate, pH 6), and 15 U catalase (5000 U/mL in PBS, pH 7.4) were added per 100 µL of saliva to deplete glucose, galactose, and the resultant hydrogen peroxide ("detection saliva"). The samples were incubated at 37°C for two hours to allow the reactions to reach completion. These clearance reactions render the assay specific for AHG as the competing substrates glucose and galactose present in the saliva are converted into species unreactive with pyranose oxidase. After incubation, the samples were transferred to Amicon ultra 3 kDa centrifugal filters and centrifuged at 14,000 g for 30 minutes to separate the enzymes from the saliva.

AHG-depleted saliva for use as a blank control ("cleared saliva") was prepared by adding 0.3 U pyranose oxidase (100 U/mL in 100 mM potassium phosphate, pH 7) per 100 µL of saliva in conjunction with 9 U glucose oxidase (3000 U/mL in 50 mM sodium acetate, pH 5), 4.5 U galactose oxidase (1500 U/mL in 100 mM potassium phosphate, pH 6), and 15 U catalase (5000 U/mL in PBS, pH 7.4) to deplete AHG, glucose, galactose, and hydrogen peroxide, respectively. The cleared samples were then incubated at 37°C for two hours—a time found in control experiments to be sufficient for the reactions to reach completion. After incubation, the samples were transferred to Amicon ultra 3 kDa centrifugal filters and centrifuged at 14,000 g for 30 minutes to separate the enzymes from the cleared saliva.

2.2.6.2. Chemiluminescent detection of AHG in saliva

Dilutions of AHG in PBS (pH 7.4) at 5, 3.75, 2.5, 1.25, and 0 µg/mL were prepared, and 10 µL of each dilution was pipetted into a single well of a white 96-well half-area microplate. 40 µL of cleared saliva was added to each well, making the final concentrations of the calibration standards 1, 0.75, 0.5, 0.25, and 0 µg/mL of AHG in cleared saliva. Additionally, 10 µL of PBS and 40 µL of detection saliva were added to three separate wells. To initiate the oxidation of AHG, 30 mU pyranose oxidase (10 U/mL in 100 mM potassium phosphate, pH 7) and 50 µL of room temperature HyPerBlu chemiluminescence reagent were added to each well, and the kinetic luminescence was immediately measured under the conditions described in the "Kinetic luminescent intensity recording" section below. The calibration curve was developed following the method described in the "Data analysis" section and plotting the calculated rate of produced luminescence of each sample against their respective AHG concentrations.

2.2.7. Kinetic luminescent intensity recording

The kinetic luminescence was measured with a Tecan Infinite M200 Pro microplate reader in luminescence mode heated to 37°C. The total duration was 30 minutes, with a one-second integration time per well.

2.2.8. Data Analysis

The intensity of the produced chemiluminescence was recorded in units of photons emitted per second (counts/s). Due to the specific properties of the HyPerBlu reagent, the amount of light produced by the chemical reaction, and hence the luminescent intensity, increases linearly with time[16]. Based on this, the rate at which the light was produced is calculated by determining the slope of the linear intensities in units of counts/s^2.

2.3 Results and discussion

2.3.1. Comparison of control and diabetic samples with initial assay protocol

To explore the potential utility of this approach, we compared the relative AHG concentration in the saliva of 55 control (i.e., not known to be diabetic) individuals and 210 diabetic patients undergoing treatment at the Clínicas del Azúcar in Monterrey, Mexico, a specialized diabetes clinic. Because it can be challenging to enroll persons with uncontrolled diabetes, the diabetic samples here are from patients actively treated for diabetes at Clínicas del Azúcar. Hence, they are less likely to have recently had significantly high blood glucose levels. The control samples are from persons self-reported as non-diabetic. Here, saliva samples were treated with glucose oxidase (100 U/mL), galactose oxidase (500 U/mL), and catalase (2000 U/mL) and incubated at 37°C

overnight to ensure complete clearance of the glucose analogs. We recorded the total luminescence intensity, proportional to the amount of AHG in the saliva, at 700 seconds after adding pyranose oxidase (2.7 U/mL) and HyPerBlu chemiluminescence reagent.

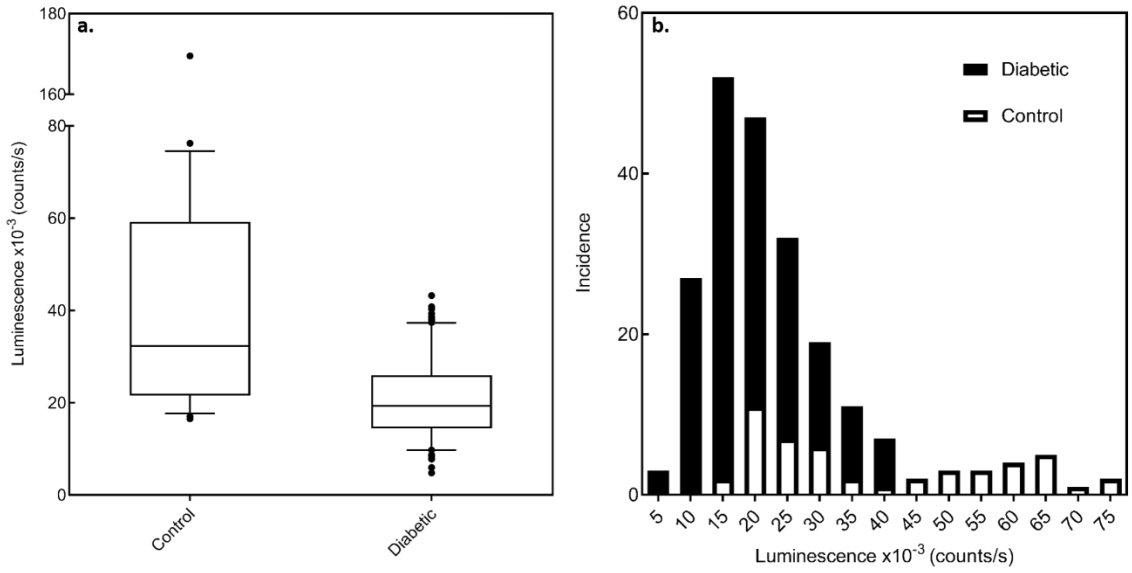

Figure 2.3. (a) Comparison of assay results with saliva of diabetics and healthy individuals (control). (b) Histogram comparison of assay results with saliva of diabetics and healthy individuals (control).

The intensity of the control samples was noticeably higher than the diabetic samples (Fig. 2.3), suggesting an ability to identify impaired AHG reuptake in even these treated diabetics. Despite some overlap between the two groups, there is a clear distinction between healthy and diabetic samples. The p-value determined by a Mann-Whitney test (GraphPad Prism version 9.1) for the null hypothesis that relative AHG concentration is comparable for healthy and diabetic saliva samples is less than 0.0001. This difference in the intensities supports that having a lower concentration of AHG in

the saliva indicates diabetic status and that this initial assay could detect the difference in intensity.

Using this assay, we developed a receiver operating characteristic (ROC) curve (Fig. 2.4), representing the potential diagnostic utility of measuring AHG concentration in saliva as a marker for diabetes. Our data suggest that this initial chemiluminescent assay for AHG in saliva is approximately 82% accurate in detecting diabetes from the area under the ROC curve. We expect the assay to be even more accurate when distinguishing between healthy individuals and untreated, undiagnosed diabetics.

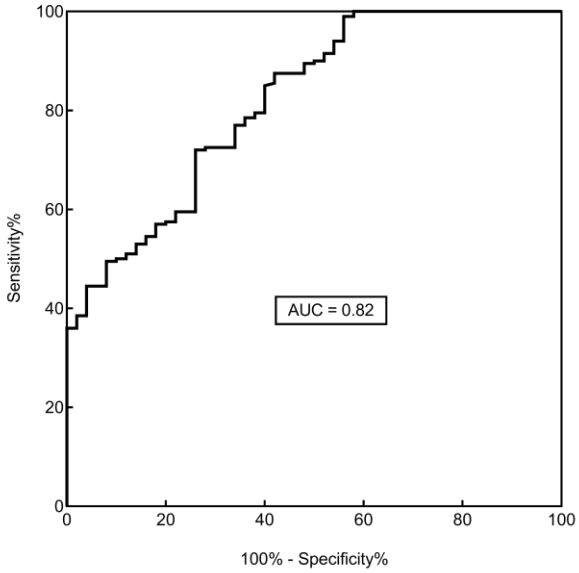

Figure 2.4. Receiver operating characteristic curve for diabetes screening by enzymatic detection of 1,5-anhydroglucitol in saliva.

2.3.2. Effects of sample collection method

Various methods and devices exist to collect human whole saliva samples[89–91]. We compared the preliminary trial results with samples collected by Salivette® cotton absorbent swab or the more economical passive drool method(Fig. 2.5). The p-value for

the null hypothesis that the assay signal is the same for saliva samples collected by Salivette and passive drool is 0.90, indicating a negligible difference in results obtained by the two collection methods.

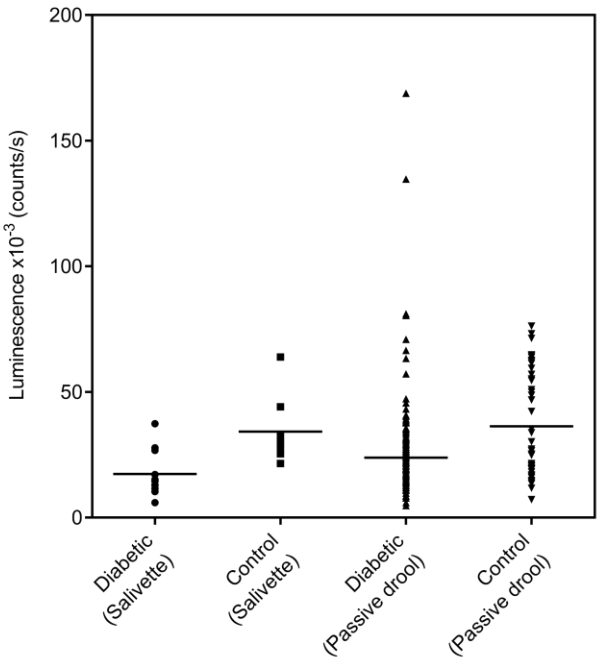

Figure 2.5. Effect of saliva collection method on assay performance for diabetic and control samples.

2.3.3. Optimization of enzymatic interferent depletion

Given our encouraging preliminary results with the saliva samples obtained from Clínicas del Azúcar and overnight clearance incubation, we sought to optimize the assay protocol by decreasing the time required for saliva pre-treatment. While the initial concentration of each interferent in saliva cannot be independently controlled, we optimized clearance by varying the enzyme concentrations and treatment time before ultrafiltration to remove the clearance enzymes. Varying concentrations of glucose

oxidase and galactose oxidase coupled with catalase were added individually to separate samples of saliva pooled from healthy individuals and incubated at 37°C for different periods to determine the lowest required enzyme concentrations and treatment duration (Fig. 2.6). The glucose oxidase or galactose oxidase added to the saliva in addition to catalase will oxidize the glucose or galactose present in the sample. The hydrogen peroxide produced by these reactions is reduced by catalase. The enzymes were then separated from the samples by 3 kDa centrifugal filtration. Following ultrafiltration, 3000 U/mL of glucose oxidase was added to the samples depleted of glucose, and 1500 U/mL of galactose oxidase was added to the galactose-depleted samples. The addition of these enzymes in the presence of a chemiluminescence reagent (HyPerBlu) will produce light if any of their respective substrates remain in the sample following clearance. For example, if the saliva hypothetically was cleared entirely of glucose or galactose, the only light produced by the sample with these enzymes will be from the background signal.

For glucose clearance, we observed that samples reached an intensity similar to the background after 60 minutes with 3000 U/mL glucose oxidase or two hours for the samples cleared with 30 or 300 U/mL glucose oxidase. The samples were fully depleted of galactose by galactose oxidase in 60 minutes for each tested concentration (15, 150, and 1500 U/mL galactose oxidase). The concentration of catalase used for each experimental condition was 5000 U/mL.

Similarly, we determined the optimal concentration and incubation time to clear saliva of AHG by pyranose oxidase so that known amounts of the sugar may be spiked into the saliva to prepare calibration standards.

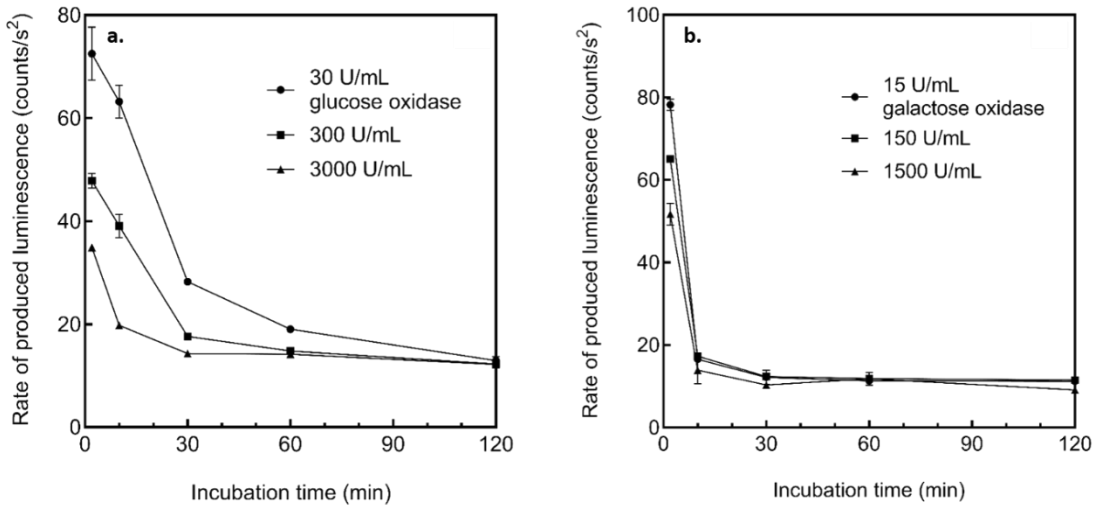

Figure 2.6. (a) Effect of incubation time and glucose oxidase concentration on glucose depletion from saliva (N = 3). (b) Effect of incubation time and galactose oxidase concentration on galactose depletion from saliva (N = 3).

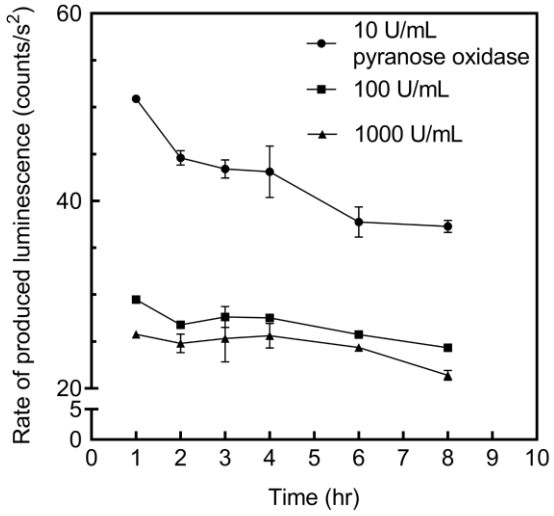

Figure 2.7. Effect of incubation time and enzyme concentration on the depletion of glucose, galactose, and AHG from saliva by glucose oxidase, galactose oxidase, and pyranose oxidase (N = 3).

Glucose and galactose oxidase were added to saliva at the previously determined optimal concentrations (3000 U/mL and 1500 U/mL, respectively) with 5000 U/mL catalase.

Additionally, various concentrations of pyranose oxidase were added to the saliva and incubated at 37°C for different periods (Fig. 2.7). Following incubation and subsequent ultrafiltration, pyranose oxidase at 10 U/mL and HyPerBlu chemiluminescent reagent were added to the samples.

Because pyranose oxidase is reactive with glucose, galactose, and AHG, saliva that is fully depleted of these compounds should have lower luminescent intensity than saliva that has not reached complete clearance. The samples treated with 100 or 1000 U/mL pyranose oxidase were cleared after two hours of incubation. However, samples treated with 10 U/mL pyranose oxidase were not cleared even after eight hours.

2.3.4. Optimized protocol and LC-MS comparison

We cross-checked the optimized assay protocol against LC-MS, described in detail in the Appendix (A.3). To measure the absolute concentration of AHG by the enzymatic assay, pooled saliva samples from a single healthy individual were cleared of glucose, galactose, and AHG using glucose oxidase, galactose oxidase, pyranose oxidase, catalase, and ultrafiltration. A calibration curve was constructed by spiking AHG at known concentrations into the cleared saliva and using pyranose oxidase and HyPerBlu to produce luminescence from the spiked AHG (Fig. 2.6). The concentration of AHG in the pooled saliva determined by the linear fit of the calibration curve was approximately 0.76 ± 0.14 μg/mL from three replicates (Fig. 2.8).

The AHG concentration of the same pooled sample was determined to be 0.64 μg/mL by Dionex IonPac ion chromatography-ESI-MS analysis (UT MD Anderson Cancer Center Proteomics Facility; Figs A.4 & A.5). While this result further supports the

method's accuracy, extensive evaluation with additional healthy and diabetic saliva samples should be performed to validate the assay fully.

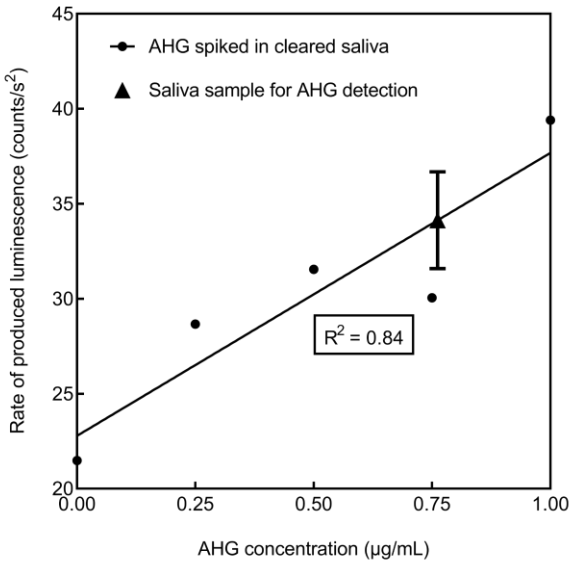

Figure 2.8. Calibration curve to quantify 1,5-anhydroglucitol concentration in saliva by the optimized enzymatic assay.

3. COMPARISON OF RAPID HUMAN IgG DETECTION BY COLORIMETRIC AND NANOPHOSPHOR LATERAL FLOW ASSAYS

3.1. Introduction

Lateral flow assays (LFAs) provide a simple, cost-effective, and rapid method to detect an analyte of interest at the level of point-of-care or -need, making their use common in biomedicine and the food and agricultural industries. Unlike other immunoassay formats like the enzyme-linked immunosorbent assay, LFAs primarily consist of membranes that contain a series of capillary beds on which antibodies are immobilized[49]. As a liquid sample flows through the capillaries, the target analyte in the sample binds to the reporter-antibody conjugate at the conjugate release pad. After conjugate release, the antigen binds to the capture antibody present at the test line, and the remaining unbound conjugates are captured at the control line.

The most widely available commercial LFA is the home pregnancy test, which commonly uses either colloidal gold or colored (blue) latex nanoparticles as its reporters[49]. As the reporter-conjugated antibody accumulates at either the LFA test or control line, a visible red or blue line will appear from the gold or blue latex nanoparticles, respectively. Lines that appear at both the test and control sites signify a positive result, and a single line at the control denotes a negative result. As these LFAs rely upon the observation of lines by the test operator, they are used solely as qualitative assays. However, the diagnosis of many common diseases, such as diabetes mellitus, anemia, or thyroid deficiencies, requires a quantitative assay that can determine the absolute concentration of the target analyte.

Quantitative LFAs that use instrument-based reporters such as up-converting phosphors, magnetic microparticles, and fluorescent labels are available. However, these LFAs often require costly laboratory equipment, defeating the purpose of a point-of-care test. We have developed strontium aluminate persistent luminescent nanoparticles (PLNPs; "nanophosphors") as LFA reporters[9]. The europium- and dysprosium-doped strontium aluminate nanophosphors ($SrAl_2O_4$: Eu^{2+}, Dy^{3+}) emit a long-lasting, bright glow upon excitation that allows for a delayed emission measurement. This delay reduces background auto-fluorescence and eliminates the need for precision optical filters. Compared to colloidal gold LFAs, strontium aluminate nanophosphor LFAs have a minimum 10-fold higher sensitivity[9]. Additionally, because this reporter system allows for smartphone imaging and analysis, the occurrence of false positives or negatives due to human error is limited[8].

Human IgG is a beneficial biomarker for various disease diagnostics, such as *Helicobacter pylori* infection, HIV, dengue virus, and SARS-CoV-2[53–56]. IgG quantification is also advantageous in a variety of other unique applications, including monitoring monoclonal antibody production and manufacturing[57]. Recently, human IgG has been proposed as a specific marker for human fecal-water contamination, suggesting that human IgG potentially serves as a single-molecule marker for rapid, one-step detection of human fecal contamination in water sources[58]. Here, we develop three LFAs using colloidal gold nanoparticles, blue latex nanoparticles, or nanophosphors to quantify total human IgG. By comparing the limit of detection of the three LFAs, we can evaluate the utility of the nanophosphor-based assay as a quantitative test and assess its potential capabilities over colorimetric LFAs.

3.2. Methods

3.2.1. Materials

Goat anti-human IgG and goat anti-human IgG-Fc antibodies were purchased from Arista Biologicals, Inc. (Allentown, PA). Donkey anti-goat IgG antibodies were purchased from Santa Cruz Biotechnology (Santa Cruz, CA). Colloidal gold 40 nm nanoparticles (OD1) and adhesive LFA backing cards were purchased from DCN Dx (Carlsbad, CA). Carboxylate-modified blue latex 400 nm nanoparticles were purchased from Thermo Fisher Scientific (Waltham, MA). Strontium aluminate Ultra Green V10 Glow-in-the-Dark Powder was purchased from Glow, Inc (Ennis, TX). A Vibro-Energy wet grinding mill (model M18-5) was purchased from SWECO (Florence, KY). Tetraethyl orthosilicate and bovine serum albumin were purchased from Sigma Aldrich (St. Louis, MO). Triethoxysilylbutyraldehyde was purchased from Gelest, Inc. (Morrisville, PA). Sodium cyanoborohydride was purchased from Chem-Impex International, Inc. (Wood Dale, IL). Whatman CF5, Standard 14, and FF80HP membranes were purchased from Cytiva Life Sciences (Marlborough, MA). Ahlstrom conjugate release pad membrane, grade 8964, was purchased from Ahlstrom-Munksjö (Helsinki, Finland). Lateral flow adhesive tape samples were obtained from the Lohmann Tape Group (Neuwied, Germany).

3.2.2. Nanophosphor preparation

Procedures for grinding, sizing, silica-coating, and antibody-conjugation of strontium aluminate PLNPs were as described previously[8], with minor modifications. Strontium aluminate powder (10 g; 5 – 15 μm diameter) was suspended in 100 mL of anhydrous ethanol and wet milled for 10 days in a grinding mill using 0.5 kg of 0.25-inch (6.35 mm) magnesia-stabilized zirconia grinding cylinders. The milled particle

suspension was dried, and the phase purity of the milled particles was confirmed with a PANalytical X'Pert powder diffractometer using Cu Kα radiation (1.54183 Å). Differential centrifugal sedimentation in anhydrous ethanol was used to isolate 200–300 nm nanophosphors[9]. The final concentration of particles was determined by thoroughly drying and weighing a small volume of the fractionated nanophosphor suspension.

3.2.3. Antibody-reporter conjugate preparation

3.2.3.1. Colloidal gold nanoparticles

Gold nanoparticles were functionalized with goat anti-human IgG antibodies by passive adsorption. 1 mL of 40 nm colloidal gold particles were incubated with 10 μg of antibody in 100 μL of 4 mM potassium chloride for 20 minutes on a 30 rpm rotator at room temperature. Following conjugation, the particles were passivated by adding 100 μL of 10% bovine serum albumin (BSA) and incubated at room temperature on a rotator at 30 rpm for an additional 20 minutes. After passivation, the gold particles were washed and then stored at 4°C in a buffer of PBS (pH 7.4), 1% BSA, and 10% sucrose.

3.2.3.2. Blue latex nanoparticles

Carboxylated blue latex particles (400 nm diameter) were prepared to 0.5% concentration in 50 mM MES buffer (pH 5.8). Following three washes with MES buffer, the carboxyl sites were activated with 23.4 μL of 10 mg/mL 1-ethyl-3-(3-dimethylaminopropyl)carbodiimide (EDC) and 18.4 μL of 50 mg/mL N-hydroxysuccinimide (NHS) in 950 μL of MES buffer for 30 minutes at room temperature on a rotator at 30 rpm. After washing and resuspending the nanoparticles in 650 μL of PBS, 350 μg of goat anti-human IgG was added. The suspension was incubated for four

hours at room temperature with rotation. After incubation, the particles were centrifuged for 10 minutes at 16,000 g, and the supernatant was discarded. The unreacted carboxylate sites were passivated with a 4% BSA solution for one hour at room temperature on a rotator at 30 rpm. The particles were then washed three times with 1% BSA in PBS and stored at 4°C in the same solution at an approximate concentration of 1% solids.

3.2.3.3. Nanophosphors

A mass of 2 mg of fractionated nanophosphors was silica-encapsulated with tetraethyl orthosilicate (TEOS) to improve water stability using a modified Stöber process as previously described[9]. Briefly, the phosphors were encapsulated using 20 mM TEOS in 81.4% ethanol in the presence of 400 mM ammonium hydroxide. Following an 8-hour incubation on a 30 rpm rotator, the now encapsulated phosphors were washed with anhydrous ethanol in preparation for silanization. Silica-encapsulated phosphors were silanized with 50 mM triethoxysilylbutyraldehyde (TESBA) in the presence of 25 mM TEOS and 93% ethanol for 12 hours on a rotator at 30 rpm to introduce surface aldehydes. After silanization, the nanophosphors were washed three times in ethanol by sonication and centrifugation at 10,000 g for 2 min. Surface aldehydes were reacted with the primary amines of 50 μg of goat anti-human IgG antibodies in the presence of 250 mM sodium cyanoborohydride and incubated on a 30 rpm rotator at room temperature for two hours. The nanophosphors were washed three times in PBS, and unreacted surface aldehydes were blocked with 3% bovine serum albumin for three hours. After blocking, the nanophosphors were washed three times with PBS and stored at 4°C in 100 μL of 10 mM sodium borate (pH 8.5), 150 mM sodium chloride, 0.1% BSA, 0.04% polyvinylpyrrolidone (PVP)-40, and 0.025% TWEEN-20.

3.2.4. Lateral flow strip assembly

The sample pad was prepared by soaking 15 cm × 18 mm of Whatman Standard 14 membrane in 2.5 mL of running buffer (0.1 M phosphate buffer pH 7.4, 1% PEG-3550, 1% BSA, 0.2% TWEEN-20, and 0.3 M sodium chloride). After soaking, the sample pad membrane was dried overnight at 55°C and subsequently stored in a Secador desiccator cabinet at 3% humidity until strip assembly. Separately, the conjugate release pad was prepared by soaking 15 cm × 10 mm of Ahlstrom 8964 membrane in 1 mL of conjugate buffer (0.01 M Tris pH 8.5, 1% BSA, 5% trehalose, 10% sucrose, 0.1% TWEEN-20, and 3 mg of colloidal gold, latex, or nanophosphors). After soaking, the conjugate pad membrane was dried overnight at 55°C and subsequently stored in a Secador desiccator cabinet at 3% humidity until strip assembly. The LFA strips were assembled on 15 cm long backing cards with an 18 mm sample pad, 10 mm conjugate release pad, 25 mm Whatman FF80HP membrane, and 18 mm of Whatman CF5 membrane as an absorbent pad with 1 – 2 mm of overlap between each membrane. Adhesive tape (10 mm) was applied to the overlapping sample and conjugate release pads to promote sample wicking.

Test and control lines consisting of 40 μL of 0.33 mg/mL of goat anti-human IgG-Fc and donkey anti-goat IgG antibodies, respectively, were striped on the cards using a BioDot XYZ3060™ Dispense System at 1 μL/cm. The fully assembled LFA cards were dried overnight at 55°C and stored for 24 hours in a 3% humidity Secador desiccant cabinet. After drying, 3 mm individual LFA strips were cut using a KinBio ZQ2000 guillotine cutter and stored in a 50 mL Falcon tube with a silica gel bead desiccant packet until later use.

3.2.5. Lateral flow assay protocol

Human IgG was diluted to 0 – 500 ng/mL in PBS (pH 7.4), and 50 μL of each sample was applied dropwise to the sample pad of individual lateral flow strips. The sample was allowed to wick up the strip on a horizontal surface for 20 minutes. LFA strips with colloidal gold or blue latex nanoparticles were imaged with an Epson Perfection V600 photo scanner. Nanophosphor LFA strips were imaged using an Alpha Innotech Corp. FluorChem-based imaging platform containing a FluorChem SP gel cabinet, two 10 W UV LED lights (395 – 400 nm wavelength, 9 – 11 V forward voltage, 900 mA forward current), and a CoolSNAP K4 CCD 2048 × 2048-pixel camera controlled by Micro-Manager 1.4.22 software. Nanophosphors captured on the LFA strips underwent photoexcitation by the UV LEDs and were imaged with a 3 s exposure time.

3.2.6. Image analysis

A custom-made software designed to determine the signal intensity at individual pixels was used to analyze the colorimetric and nanophosphor LFA strips. The software was used to generate a plot profile of pixel intensities as a function of position along the LFA membranes. The area of the peaks located at the test and control lines were defined as the test line signal and control line signal, respectively. We calculated the related signal of the test line as the ratio of the test-to-control line signals.

3.3. Results and discussion

3.3.1. Colloidal gold

A serial dilution series of human IgG concentrations from 0 – 500 ng/mL were tested in triplicate using a colloidal gold-nanoparticle lateral flow assay (Fig. 3.1,

replicates in Fig. B.1). As expected, higher concentrations of IgG resulted in a more robust and brighter red color at the anti-human IgG test line than those of lower IgG concentration. ImageJ was used to determine the relative colorimetric intensities of the test and control lines (Fig. 3.2). The peaks of the test and control line are uncharacteristically bimodal, likely due to the coffee ring effect, in which the antibodies accumulate at the outer edges of the lines. A standard curve was developed from the ratios of test-to-control line area under the curves (Fig. 3.3). The curve is nearly linear, with only discrepancies at the highest and lowest analyte concentrations. The limit of detection (LOD) of the colloidal gold nanoparticle LFA (taken as the average of the negative control plus three times its standard deviation) is approximately 50.8 ng/mL human IgG as determined from the standard curve.

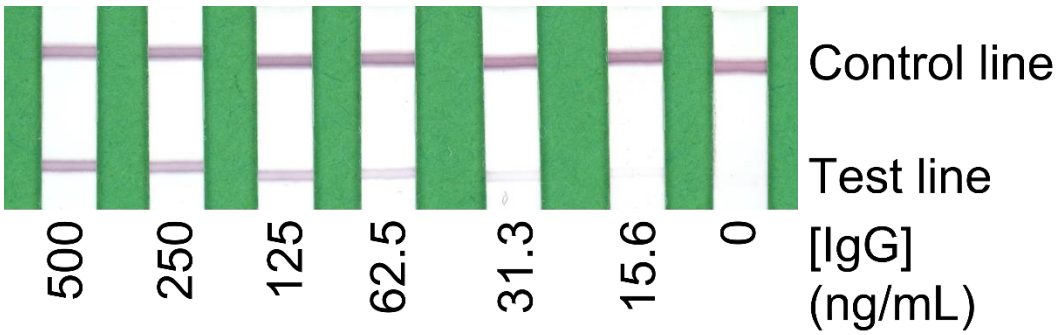

Figure 3.1. Detection of human IgG by a colloidal gold nanoparticle lateral flow assay.

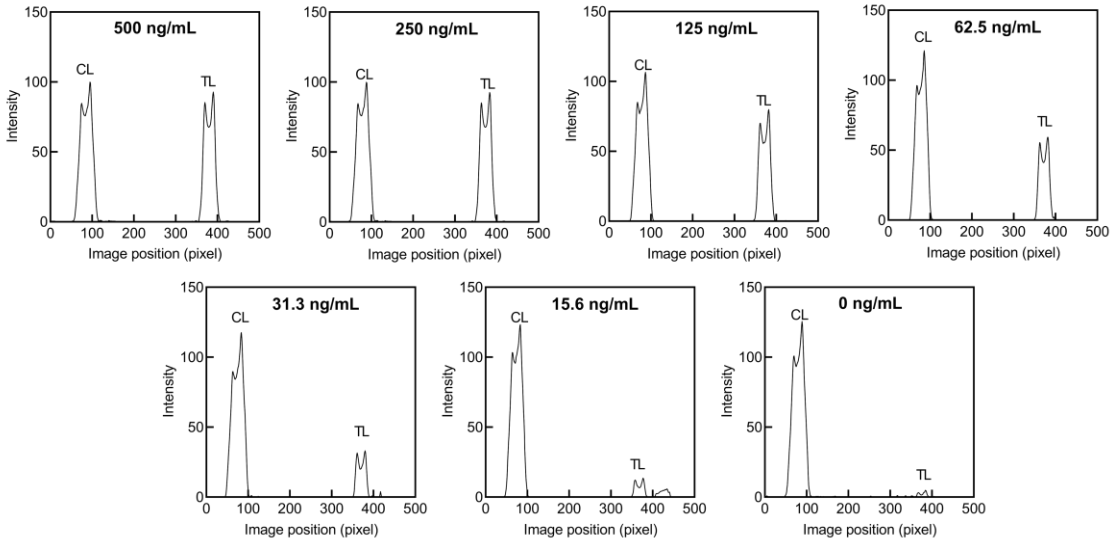

Figure 3.2. Image analysis showing the relative colorimetric intensities at the test and control lines of the colloidal gold nanoparticle lateral flow assay for varying concentrations of human IgG.

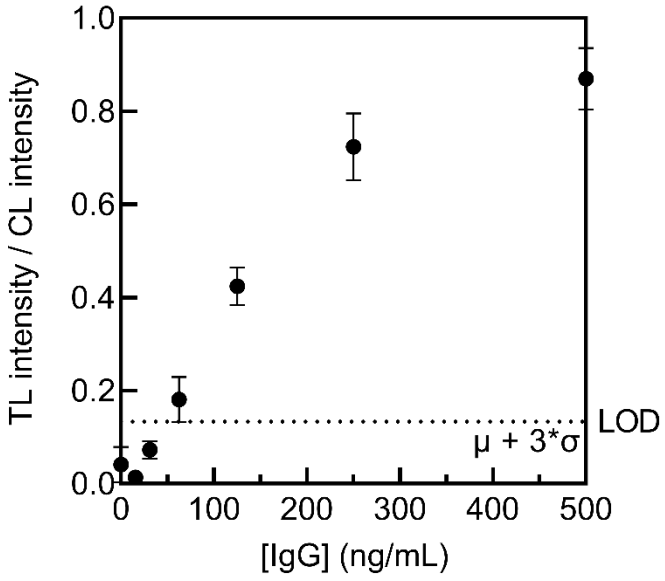

Figure 3.3. Standard curve for the colloidal gold nanoparticle lateral flow assay showing the relationship between the ratio of test to control line colorimetric intensity and human IgG concentration.

3.3.2. Blue latex nanoparticles

Like the colloidal gold nanoparticle LFA, the LFA using blue latex nanoparticles showed a brighter, more vivid blue color at the anti-human IgG test line when there were higher concentrations of IgG in the test sample (Fig 3.4, replicates in Fig. B.2). However, the colorimetric intensity of both the test and control lines of the 500 and 250 ng/mL LFA strips are visibly lower, as confirmed by the ImageJ analysis (Fig. 3.5). This may be due to the hook effect, in which excess analyte prevents the formation of the antibody sandwich between the capture and detection antibodies. Additionally, there is a visible defect in the control line of the negative sample, which was likely the result of a striping error during the LFA assembly.

Like the colloidal gold nanoparticle LFA, the standard curve of the LFA with blue latex nanoparticles is mostly linear when excluding the highest analyte concentrations (Fig. 3.6). The limit of detection (the average signal of the negative control plus three times its standard deviation) of human IgG by the blue latex nanoparticle LFA is 36.4 ng/mL.

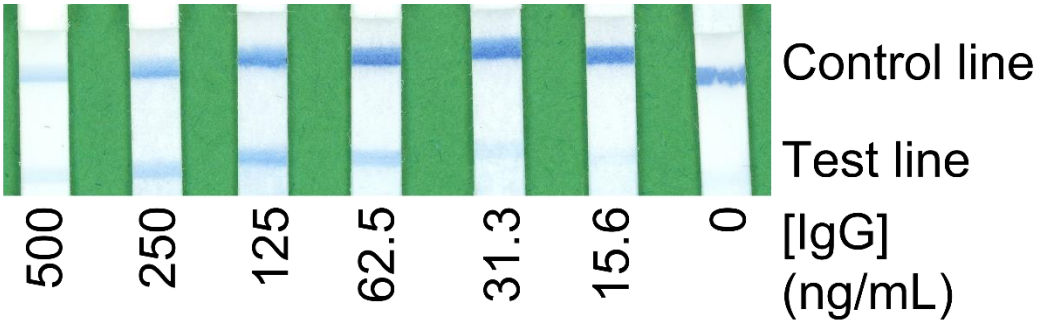

Figure 3.4. Detection of human IgG by a blue latex nanoparticle lateral flow assay.

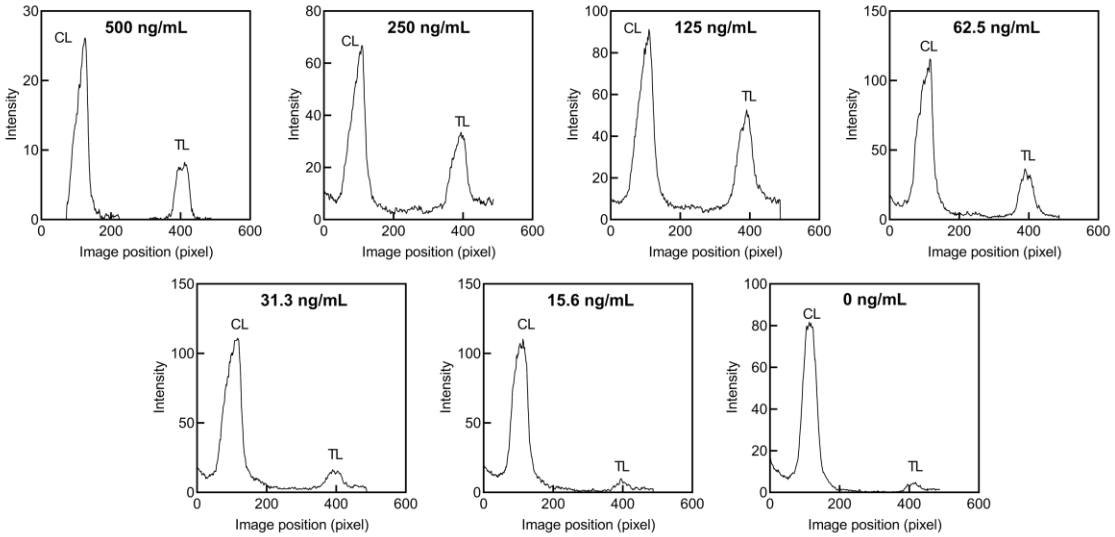

Figure 3.5. Image analysis showing the relative colorimetric intensities at the test and control lines of the blue latex nanoparticle lateral flow assay for varying concentrations of human IgG.

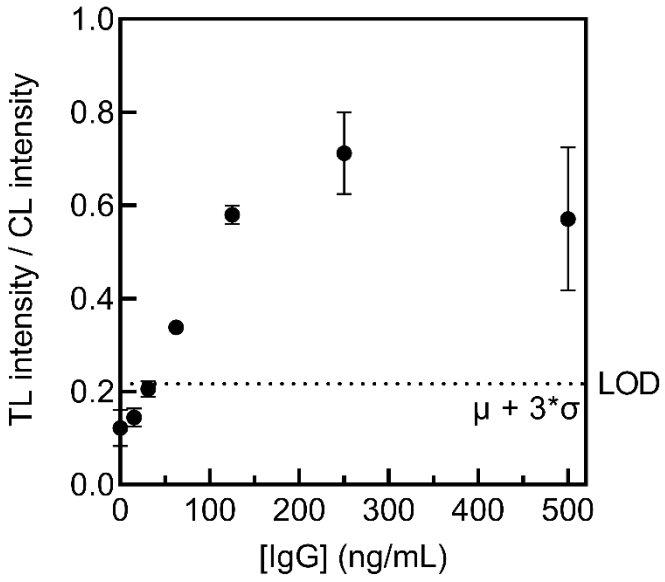

Figure 3.6. Standard curve for the blue latex nanoparticle lateral flow assay showing the relationship between the ratio of test to control line colorimetric intensity and human IgG concentration.

3.3.3. Nanophosphors

Unlike the colloidal gold and blue latex nanoparticle-based LFAs, the LFA utilizing the nanophosphor reporters can quantitatively measure the amount of human IgG in a liquid sample. Nanophosphors produce a persistent luminescent light signal when excited, allowing the LFA test strips to be imaged and analyzed to determine the luminescent intensity at specific points along the strip. The ratio of the luminescence observed at the test line to the control line can then be used to develop a standard curve to calculate unknown concentrations of the target analyte.

Human IgG ranging from 0 – 10 ng/mL in PBS were tested in triplicate using the nanophosphor-based LFA and imaged by FluorChem (Figure 3.7, replicates in Fig. B.3). Strong test and control lines were observed for most tested samples, with the test line intensity decreasing for samples less than 1.25 ng/mL human IgG. Some non-specific binding of the antibody-nanophosphor conjugate was observed at the test line of the negative control.

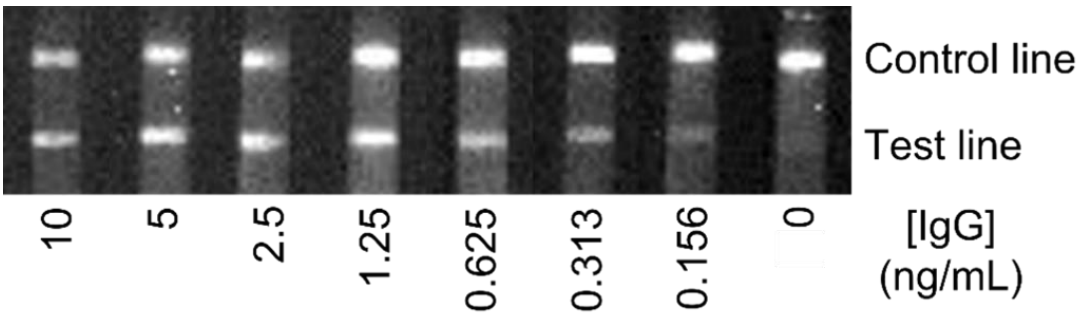

Figure 3.7. Detection of human IgG by a persistent luminescence nanophosphor lateral flow assay.

The luminescent intensities of the test and control lines of the nanophosphor LFA tested with the serial dilution of human IgG were analyzed using ImageJ (Fig. 3.8). The ratio of the test to control line intensity was determined from the area under the peaks given by the test and control lines from the ImageJ analysis. A standard curve was developed from these ratios comparing the test to control line luminescent intensity against their respective human IgG concentrations (Fig. 3.9). The limit of detection, defined here as the average signal of the negative control plus three times its standard deviation, was under 0.625 ng/mL, an 81-fold improvement over the colloidal gold LFA and a 58-fold improvement over the blue latex nanoparticle LFA. This result confirms the utility of the nanophosphor LFA and the advantage over its colorimetric competitors.

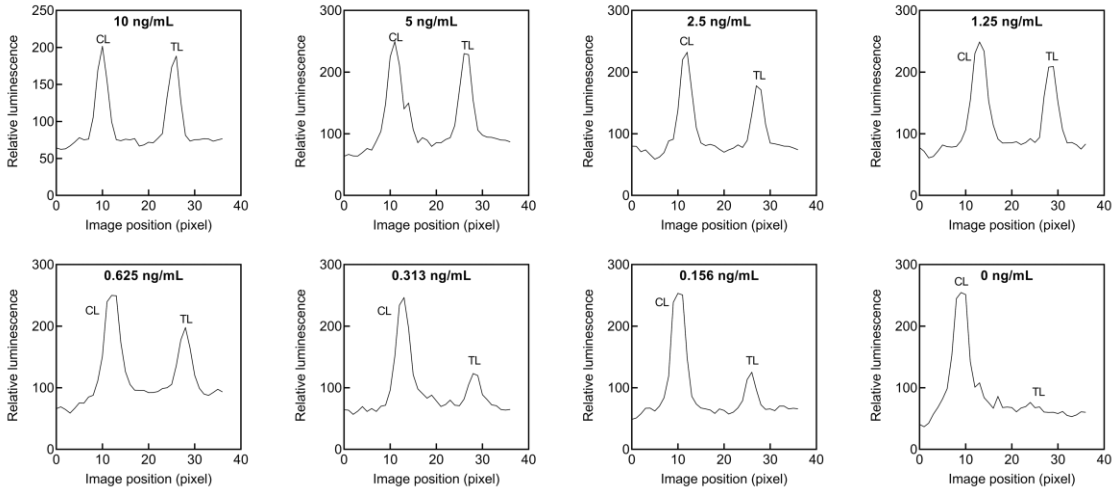

Figure 3.8. Image analysis showing the relative luminescent intensities at the test and control lines of the nanophosphor lateral flow assay for varying concentrations of human IgG.

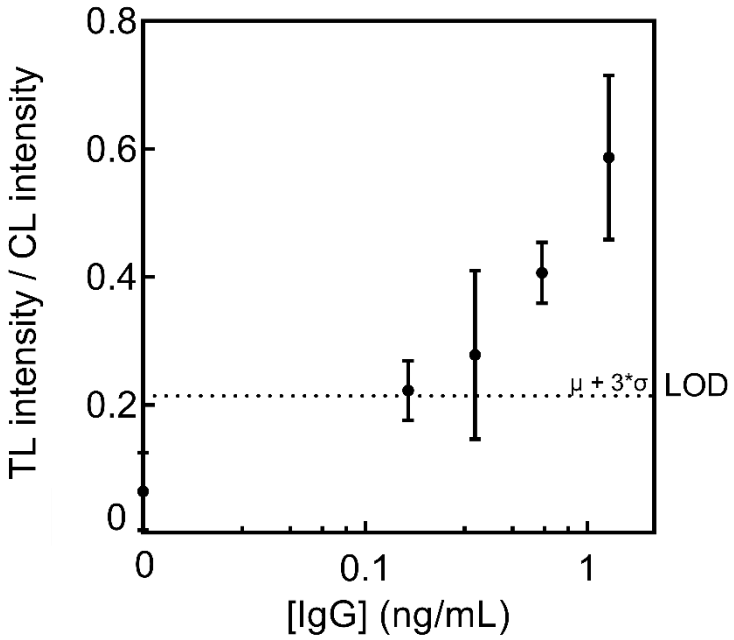

Figure 3.9. Standard curve for the nanophosphor lateral flow assay showing the relationship between the ratio of test to control line luminescent intensity and human IgG concentration (N = 3).

4. SENSITIVE DETECTION OF DENGUE NS1 BY NANOPHOSPHOR LATERAL FLOW IMMUNOASSAY

4.1. Introduction

Dengue is a systemic mosquito-borne viral disease that can cause severe, flu-like illness in infected individuals. Classified as a neglected tropical disease, dengue is endemic in over 120 countries, affecting approximately 390 million people per year[92]. Four distinct dengue virus (DENV) serotypes exist, all known to cause infection[63]. Consequently, subsequent infection by a different DENV serotype can lead to severe complications, such as plasma leakage, pulmonary effusion, cardiac arrest, and organ failure, due to antibody-dependent enhancement[93]. Severe dengue is responsible for 40,000 deaths worldwide per year[94]. Hence, early and accurate diagnosis is crucial for appropriate management to minimize the development of severe dengue.

In endemic areas, dengue is commonly diagnosed clinically based on symptoms and physical examination[68,69]. However, because DENV infection is symptomatically similar to many other prevalent tropical diseases, especially in early infections, dengue is frequently misdiagnosed[95]. Several traditional laboratory diagnostics, including reverse transcriptase-polymerase chain reaction (RT-PCR) and enzyme-linked immunosorbent assays (ELISA), are available[69]. While highly specific, these assays may lack the sensitivity to detect early dengue infections and are often laborious and costly, making them unsuitable for use in endemic areas.

DENV non-structural protein 1 (NS1) is a pathogen-specific antigen that has been found to strongly correlate with viral load, allowing its use as a marker of acute-phase dengue[96]. Accordingly, NS1 detection in blood sera or tissue specimens is a validated

diagnostic method for early dengue infection[97]. Commercial dengue lateral flow assays (LFA) are available. However, commercial LFAs generally lack the sensitivity required to detect clinically relevant concentrations of NS1[98]. Incorporating a heat-mediated immune-complex dissociation (ICD) sample pre-treatment step and using monoclonal antibodies (mAbs) specific to the monomeric form of NS1 can significantly improve NS1 rapid test sensitivity[99]. In addition, most commercial dengue LFAs use colorimetric colloidal gold nanoparticle reporters. Instrument-based reporters such as up-converting phosphors, magnetic microparticles, and fluorescent labels support more sensitive LFAs. However, these assays often require costly laboratory equipment, defeating the purpose of a point-of-care test. We have developed strontium aluminate persistent luminescent nanoparticles (PLNPs; "nanophosphors") as LFA reporters[9]. Upon light excitation, the europium- and dysprosium-doped strontium aluminate nanophosphors ($SrAl_2O_4$: Eu^{2+}, Dy^{3+}) emit a long-lasting, bright glow that allows for a delayed emission measurement, reducing background auto-fluorescence and eliminating the need for precision optical filters. Strontium aluminate nanophosphor LFAs have at minimum 10-fold higher sensitivity over colloidal gold LFAs[9]. Additionally, this reporter system allows for smartphone imaging and analysis, limiting the occurrence of false positives or negatives due to human error[8].

Here we utilize nanophosphor lateral flow technology combined with monoclonal antibodies specific to DENV NS1 to enhance the sensitivity of currently available DENV NS1 rapid tests. We have developed a nanophosphor-based LFA with a smartphone reader to detect low concentrations of NS1 and compare its sensitivity to an analogous NS1 capture ELISA.

4.2. Methods

4.2.1. Materials

Mouse anti-NS1 monoclonal antibody cell culture harvests (2G1 and 4G3) were prepared at the Centers for Disease Control and Prevention in Atlanta, GA. Goat anti-mouse IgG antibodies were purchased from Santa Cruz Biotechnology (Santa Cruz, CA). DENV NS1 serotype 1 was purchased from The Native Antigen Company (Oxford, United Kingdom). Zeba™ Spin Desalting Columns, 7K MWCO, 0.5 mL, 1-Step™ Ultra TMB-ELISA substrate solution, and an EZ-Link™ Sulfo-NHS-Biotin kit were purchased from Thermo Fisher Scientific (Waltham, MA). Strontium aluminate Ultra Green V10 Glow in the Dark Powder was purchased from Glow, Inc (Ennis, TX). A Vibro-Energy wet grinding mill (model M18-5) was purchased from SWECO (Florence, KY). Tetraethyl orthosilicate and bovine serum albumin were purchased from Sigma Aldrich (St. Louis, MO). Triethoxysilylbutyraldehyde was purchased from Gelest, Inc. (Morrisville, PA). Sodium cyanoborohydride was purchased from Chem-Impex International, Inc. (Wood Dale, IL). Protein G Sepharose 4 Fast Flow, chromatography columns, Whatman CF5, Standard 14, and FF80HP membranes were purchased from Cytiva Life Sciences (Marlborough, MA). Lateral flow cartridges were purchased from DCN Diagnostics (Carlsbad, CA; part no. MICA-125)

4.2.2. Protein G monoclonal antibody purification

Mouse anti-NS1 monoclonal antibodies were purified by protein G chromatography in a 0.58 mL column. All respective flow rates were 0.5 mL/min. The column was first equilibrated with 5 mL of PBS (pH 7.4). Following equilibration, cell culture harvest that had been previously filtered using a 0.22 μm syringe filter was loaded

into the column, then washed with 5 mL of PBS. Monoclonal anti-NS1 antibodies were eluted with 5 mL of 0.1 M glycine (pH 3). Immediately following elution, the antibody solutions were equilibrated with PBS using a Zeba™ 7K desalting column that had previously been washed three times with PBS. The approximate concentrations of the total protein in the antibody solutions were determined by UV absorbance using a Thermo Fisher Scientific Nanodrop 1000.

4.2.3. NS1 capture ELISA

Monoclonal mouse anti-NS1 (2G1) antibodies were biotinylated using EZ-Link™ Sulfo-NHS-Biotin as the NS1 capture ELISA detection antibodies. Per the kit instructions, NHS-biotin was added in 20-fold molar excess to 1 mg/mL of 2G1 and incubated for 2 hours at room temperature. Following biotinylation, the antibodies were equilibrated with PBS using a Zeba™ 7K desalting column that had previously been washed three times with PBS.

The NS1 capture ELISA protocol was adapted from a previously published work with slight modifications[99]. The wash buffer was composed of 0.1% TWEEN-20 in PBS, pH 7.4. Washing steps were included before the addition of any new reagents. BSA (2% in PBS) was used for blocking and to dilute the sample and detection antibody solutions. All incubations were for one hour at 37°C unless otherwise specified.

The wells of a transparent 96-well plate were coated with 10 μg/mL of monoclonal mouse anti-NS1 (4G3) antibodies diluted in PBS by overnight incubation at 4°C. After coating the wells with the capture antibody, empty sites were blocked with blocking buffer and incubation. Following blocking, NS1 antigen concentrations ranging from 0 – 100 ng/mL in blocking buffer were added to the wells and incubated. After the

NS1 capture, 2 μg/mL of biotinylated 2G1 antibodies diluted in blocking buffer was added to the wells and incubated. Streptavidin-HRP at 2 μg/mL was added to the wells and incubated. Finally, neat one-step TMB chromogenic substrate (with hydrogen peroxide) was added to the wells and allowed to react at room temperature. After 15 minutes, 100 μL of 2.5 M sulfuric acid was added, and the absorbance at 450 nm was read using a TECAN Infinite M200 Pro plate reader.

4.2.4. Nanophosphor preparation

Procedures for grinding, sizing, silica-coating, and antibody-conjugation of strontium aluminate PLNPs were as described previously[8], with minor modifications. Strontium aluminate powder (10 g; 5 – 15 μm diameter) was suspended in 100 mL of anhydrous ethanol and wet milled for 10 days in a grinding mill using 0.5 kg of 0.25-inch (6.35 mm) magnesia-stabilized zirconia grinding cylinders. The milled particle suspension was dried, and the phase purity of the milled particles was confirmed with a PANalytical X'Pert powder diffractometer using Cu Kα radiation (1.54183 Å). Differential centrifugal sedimentation in anhydrous ethanol was used to isolate 200–300 nm nanophosphors[9]. The final concentration of particles was determined by thoroughly drying and weighing a small volume of the fractionated nanophosphor suspension.

4.2.5. Nanophosphor bioconjugation

A mass of 2 mg of fractionated nanophosphors was silica-encapsulated with tetraethyl orthosilicate (TEOS) to improve water stability using a modified Stöber process as previously described[9]. Briefly, the phosphors were encapsulated using 20 mM TEOS in 81.4% ethanol in the presence of 400 mM ammonium hydroxide. Following an

8-hour incubation at room temperature on a 30 rpm rotator, the now encapsulated phosphors were washed with anhydrous ethanol in preparation for silanization. Silica-encapsulated phosphors were silanized with 50 mM triethoxysilylbutyraldehyde (TESBA) in the presence of 25 mM TEOS and 93% ethanol for 12 hours on a rotator at 30 rpm to introduce surface aldehydes. The nanophosphors were washed three times in ethanol following silanization by sonication and centrifugation at 10,000 x g for 2 min. Surface aldehydes were reacted with the primary amines of 50 μg of 2G1 monoclonal antibodies in the presence of 250 mM of sodium cyanoborohydride and incubated on a 30 rpm rotator at room temperature for two hours. The nanophosphors were washed three times in PBS buffer after antibody conjugation. Unreacted surface aldehydes were then blocked with 3% bovine serum albumin (BSA) for three hours. After blocking, the nanophosphors were washed three times with PBS buffer and stored until needed at 4°C in 100 μL of 10 mM sodium borate (pH 8.5), 150 mM sodium chloride, 0.1% BSA, 0.04% polyvinylpyrrolidone (PVP)-40, and 0.025% TWEEN-20.

4.2.6. Lateral flow strip assembly

The LFA strips were assembled on 15 cm long backing cards with a 21 mm Whatman Standard 14 membrane sample pad, 25 mm Whatman FF80HP membrane, and 23 mm of Whatman CF5 membrane as an absorbent pad with 1 – 2 mm of overlap between each membrane. Test and control lines consisting of 40 μL of 1 mg/mL monoclonal 4G3 and goat anti-mouse IgG antibodies, respectively, were striped on the cards using a BioDot XYZ3060™ Dispense System at 1 μL/cm. The fully assembled LFA cards were dried overnight at 55°C and stored for 24 hours in a 3% humidity Secador desiccant cabinet. After drying, 3 mm individual LFA strips were cut using a

KinBio ZQ2000 guillotine cutter and stored in a 50 mL Falcon tube with a silica gel bead desiccant packet until later use.

4.2.7. NS1 lateral flow assay protocol

DENV serotype 1 NS1 (5 μL) was heated to 95°C for five minutes to simulate immune complex dissociation, then diluted to 0 – 100 ng/mL in running buffer (10 mM HEPES, 0.1% PEG-3350, 150 mM sodium chloride, 0.2% TWEEN-20, and 0.25% BSA), and 50 μL of the diluted NS1 was mixed with 3 μL (60 μg) of the conjugated nanophosphors and added dropwise to the sample pad of a lateral flow strip. After 15 minutes, the strip was washed by adding 30 μL of running buffer to the sample pad. After 10 minutes, the strips were imaged by either FluorChem Imager or iPhone 5s

4.2.8. Lateral flow strip imaging

4.2.8.1. FluorChem

LFA strips were imaged using an Alpha Innotech Corp. FluorChem-based imaging platform containing a FluorChem SP gel cabinet, two 10 W UV LED lights (395 – 400 nm wavelength, 9 – 11 V forward voltage, 900 mA forward current), and a CoolSNAP K4 CCD 2048 × 2048-pixel camera controlled by Micro-Manager 1.4.22 software. Nanophosphors captured on the LFA strips underwent photoexcitation by the UV LEDs and were imaged with a 10 s exposure time.

4.2.8.2 iPhone 5s

LFA strips were also imaged using an iPhone 5s with a custom 3D printed attachment to hold an LFA test cartridge. Photoexcitation and image capture was initiated by the Luminostics™ smartphone app (Clip Health™, formerly Luminostics, Inc.). The nanophosphors were exposed to the iPhone 5s torch for 3 seconds, and four images were

captured following a 100 ms delay after the torch was switched off. The app then displayed the average result of the four images.

4.2.9. Image analysis

A custom-made software designed to determine the signal intensity at individual pixels was used to analyze the FluorChem- and iPhone 5s-imaged LFA strips. The software was used to generate a plot profile of pixel intensities as a function of position along the LFA membranes. The area of the peaks located at the test and control lines were defined as the test line signal and control line signal, respectively. We calculated the related signal of the test line as the ratio of the test-to-control line signals.

4.3. Results and discussion

4.3.1. NS1 quantification by ELISA

Because the ELISA is the gold standard for detecting DENV NS1, we prepared an ELISA analogous to our NS1 LFA to compare sensitivities. Here, the capture antibodies of the ELISA are the 4G3 mouse monoclonal antibodies, and the detection antibodies are biotinylated 2G1 mouse monoclonal antibodies to coincide with the LFA (Fig. 4.1). The limit of detection of the ELISA (average of the zero concentration plus three times its standard deviation) was 1 ng/mL from the standard curve (Figure 4.2).

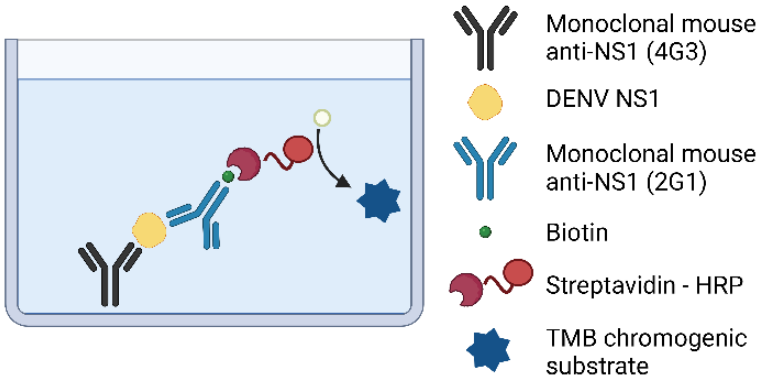

Figure 4.1. Schematic of the dengue virus non-structural protein 1 sandwich ELISA. Created with BioRender.com.

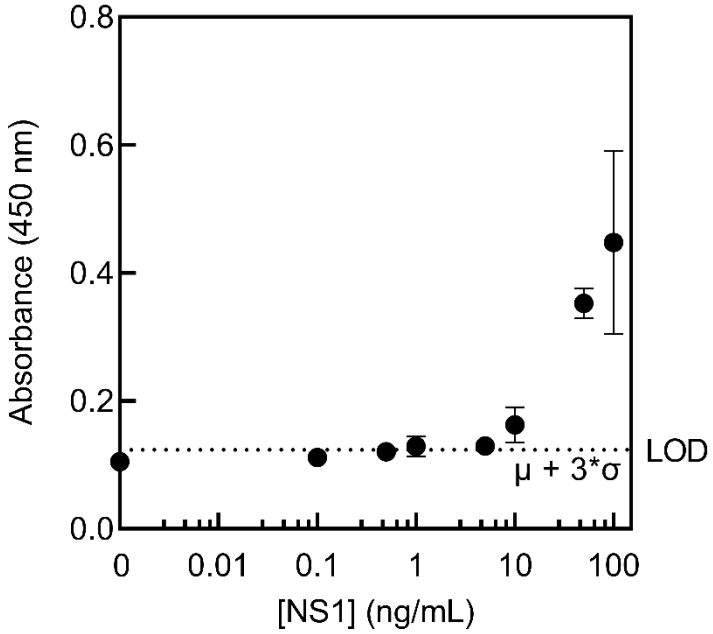

Figure 4.2. Standard curve of the dengue virus non-structural protein 1 sandwich ELISA (N = 3, some error bars are occluded by the points).

4.3.2. NS1 quantification by nanophosphor lateral flow assay

A serial dilution of DENV NS1 at concentrations from 0 – 100 ng/mL was tested in triplicate using the nanophosphor-based lateral flow assay (Fig. 4.3).

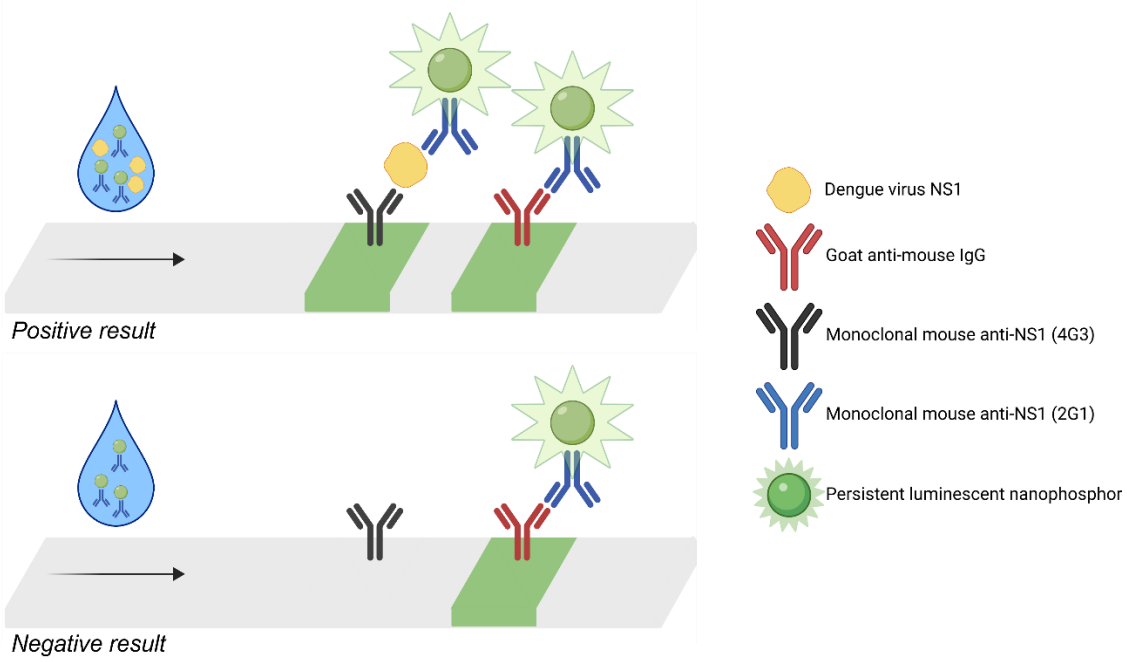

Figure 4.3. Dengue virus non-structural protein 1 lateral flow assay schematic of a positive (top) and negative (bottom) result. Created with BioRender.com.

As with the ELISA, dilutions of NS1 in buffer were first heated to 95°C to simulate heat-mediated immune complex dissociation. The run strips were imaged by either FluorChem or iPhone 5s and analyzed to determine the luminescent intensity of the test and control lines using ImageJ (Figs. 4.4 & 4.5, replicates in Figs. C.1 & C.2).

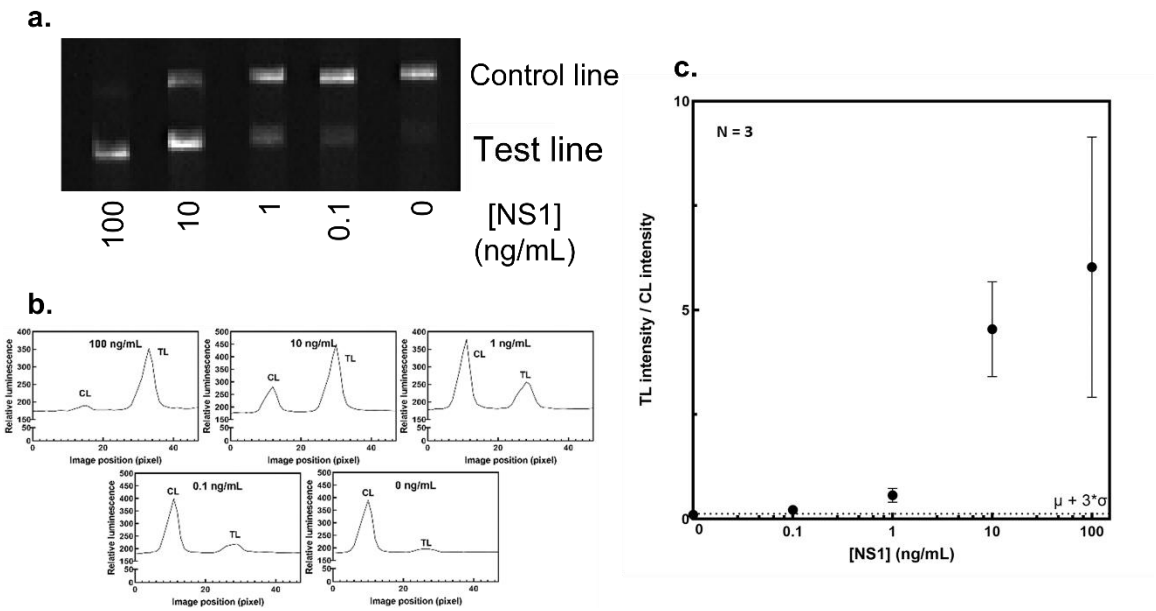

Figure 4.4. (a) FluorChem detection of dengue virus non-structural protein 1 by nanophosphor lateral flow assay. (b) Test and control line luminescent intensity analysis. (c) Standard curve of non-structural protein 1 quantification (N = 3).

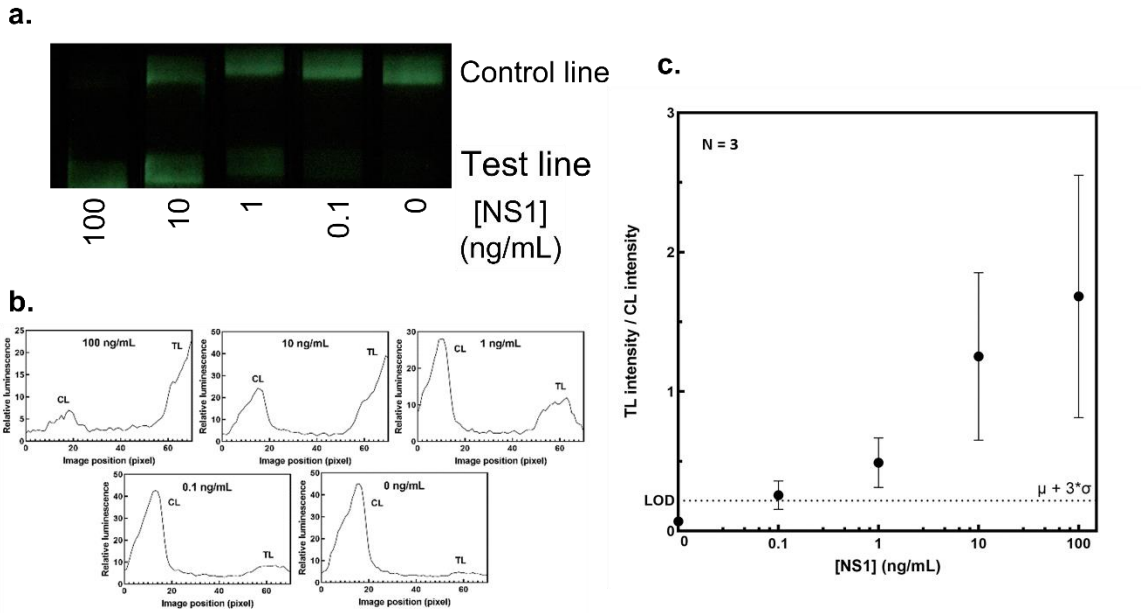

Figure 4.5. (a) iPhone 5s detection of dengue virus non-structural protein 1 by nanophosphor lateral flow assay. (b) Test and control line luminescent intensity analysis. (c) Standard curve of non-structural protein 1 quantification (N = 3).

For both sets of strips imaged by FluorChem and iPhone 5s, high concentrations of DENV NS1 caused the control line to be visibly faint with less luminescent intensity (Figs 4.4a & 4.5a). This is likely due to the overwhelming amount of NS1 present in the sample that binds to much of the mouse anti-NS1-nanophosphor conjugates, leaving very little of the antibody-reporter conjugate to bind to the anti-mouse IgG antibodies at the control line. Additionally, due to the coffee ring effect in which the test and control antibodies dry non-symmetrically during LFA strip assembly, there is visually higher luminescence at the lower portion of both the test and control lines of the strips. However, because the luminescent intensity of the lines is analyzed vertically on the strip, we can analyze the overall peak luminescence at the test and control lines (Figs 4.4b & 4.4b).

Standard curves for the quantification of DENV NS1 in buffer were developed from the ratio of the area under the luminescent intensity peaks of the test line to the control line against their respective NS1 concentrations (Figs 4.4c & 4.4c). The limit of detection (calculated by the average of the negative control plus three times its standard deviation) of NS1 by both FluorChem and iPhone 5s was approximately 1 ng/mL, confirming both the utility of the nanophosphor-based assay and the iPhone 5s imaging method.

5. CONCLUSIONS AND FUTURE WORK

5.1. Diabetes mellitus screening by chemiluminescent enzymatic detection of 1,5-anhydroglucitol in saliva

The societal burden of diabetes is heavy enough that early diagnosis is relevant not only for patient outcomes but also for societal well-being and healthcare economics. Since 1980, the number of adults with diabetes has increased dramatically from 108 million to more than 460 million in 2019, making the disease prevalence over 9% of adults worldwide[75]. Approximately 50% of diabetes cases are undiagnosed (i.e., individuals unaware that they have the condition)[75]. The total direct cost of diabetes care (emergency and inpatient hospital care, medications, medical supplies, and long-term care) exceeds 800 billion US dollars[33,34]. National and global programs have been organized to prevent and detect diabetes in vulnerable populations and delay disease progression in those already diagnosed[35,36]. Several core functions of these programs relate directly to developing and standardizing the surveillance and diagnosis of diabetes, emphasizing the importance of early detection of the disease.

We report the initial development and optimization of a chemiluminescent assay to screen for diabetes mellitus using saliva. We have validated the assay's ability to quantify AHG in whole saliva collected by two different methods and its ability to distinguish between healthy and treated diabetic individuals ($p < 0.0001$). We speculate that undiagnosed diabetics will be identified by the assay more effectively.

Although blood AHG is relatively insensitive to diet, it is unknown what effects various foods or behaviors may have on the composition of saliva and salivary AHG[76]. Several other factors, such as from which gland the saliva originates, salivary flow rate,

and oral hygiene, have been shown to influence saliva composition[100]. Therefore, a diverse study spanning several different ethnicities and cultures is required to fully understand how AHG concentration in the saliva is affected by such factors.

5.2. Comparison of rapid human IgG detection by colorimetric and nanophosphor lateral flow assays

Lateral flow assays (LFAs) are an extremely valuable and often underutilized technology for the rapid detection of proteins, DNA, RNA, and small molecules. One possible explanation for this underutilization is the lack of commercially available ultra-sensitive and quantitative LFAs. We explored the utility of three reporter systems to detect total human IgG by LFA. Two of the reporter systems, colloidal gold and blue latex nanoparticles, are commonly used in commercial LFAs and are notoriously known to have poor sensitivity. Additionally, colloidal gold and blue latex LFAs are mostly purely colorimetric and not easily quantitative, contributing to their lack of sensitivity. Conversely, persistent luminescence nanophosphors, due to their photoluminescence and extended light production, are both quantitative and highly sensitive.

Human IgG detection is the primary function of numerous medical and industrial processes, including disease diagnostics and monitoring of monoclonal antibody production, among other unique applications. We have demonstrated that the colorimetric IgG LFAs have a limit of detection of approximately 50.8 and 36.4 ng/mL for the colloidal gold and blue latex assays, respectively, and 0.625 ng/mL for the nanophosphor-based IgG LFA.

A critical distinction of colorimetric LFAs is that not all visual reporters possess poor sensitivity. Recently, colorimetric reporters such as gold nanoshells and nanorods

have shown increased sensitivity over conventional gold nanoparticles due to their improved optical properties[101,102]. Comparing these particles to nanophosphors is necessary to determine their true utility.

5.3. Sensitive detection of dengue NS1 by nanophosphor lateral flow immunoassay

Dengue fever is a neglected tropical disease that infects millions of people in Southeastern Asia, South America, and Africa. However, many of the reliable diagnostic tests available for dengue are inaccessible in these regions due to their expense and the need for highly trained operators. LFAs offer an inexpensive and simple alternative to conventional dengue diagnostic methods. However, currently available commercial LFAs for dengue lack the sensitivity to diagnose early infection.

We have developed a persistent luminescence nanophosphor-based LFA to detect dengue virus (DENV) non-structural protein 1 (NS1). DENV NS1 is a dengue-specific biomarker detectable in the early stages of infection. By utilizing heat-mediated immune complex dissociation and nanophosphor reporters, we speculate that the LFA will be able to detect early dengue infections. In buffer, the assay's limit of detection is 1 ng/mL when imaged with both a FluorChem system and an iPhone 5s.

We have only tested the LFA with DENV NS1 diluted in buffer until now. Extensive experimentation with blood specimens spiked with NS1 is required to determine the actual limit of detection of the assay. Additionally, alternative methods of immune complex dissociation should be explored to determine the optimal method to separate the antigen-antibody complex, as the current protocol of heating to 95°C for five minutes may not be sufficient.

REFERENCES

(1) pamela.corey@nist.gov. Spectrophotometry https://www.nist.gov/programs-projects/spectrophotometry (accessed 2022 -03 -14).

(2) Trumbo, T. A.; Schultz, E.; Borland, M. G.; Pugh, M. E. Applied Spectrophotometry: Analysis of a Biochemical Mixture. *Biochem. Mol. Biol. Educ.* **2013**, *41* (4), 242–250. https://doi.org/10.1002/bmb.20694.

(3) Ninfa, A. J.; Ballou, D. P.; Benore, M. *Fundamental Laboratory Approaches for Biochemistry and Biotechnology*; John Wiley & Sons: Hoboken, N.J., 2009.

(4) Fluorometer. In *Compendium of Biomedical Instrumentation*; John Wiley & Sons, Ltd, 2020; pp 823–827. https://doi.org/10.1002/9781119288190.ch152.

(5) Lakowicz, J. R. *Principles of Fluorescence Spectroscopy*; New York : Kluwer Academic/Plenum, 1999.

(6) Adan, A.; Alizada, G.; Kiraz, Y.; Baran, Y.; Nalbant, A. Flow Cytometry: Basic Principles and Applications. *Crit. Rev. Biotechnol.* **2017**, *37* (2), 163–176. https://doi.org/10.3109/07388551.2015.1128876.

(7) Quesada-González, D.; Merkoçi, A. Nanoparticle-Based Lateral Flow Biosensors. *Biosens. Bioelectron.* **2015**, *73*, 47–63. https://doi.org/10.1016/j.bios.2015.05.050.

(8) Paterson, A. S.; Raja, B.; Mandadi, V.; Townsend, B.; Lee, M.; Buell, A.; Vu, B.; Brgoch, J.; Willson, R. C. A Low-Cost Smartphone-Based Platform for Highly Sensitive Point-of-Care Testing with Persistent Luminescent Phosphors. *Lab. Chip* **2017**, *17* (6), 1051–1059. https://doi.org/10.1039/c6lc01167e.

(9) Paterson, A. S.; Raja, B.; Garvey, G.; Kolhatkar, A.; Hagström, A. E. V.; Kourentzi, K.; Lee, T. R.; Willson, R. C. Persistent Luminescence Strontium

Aluminate Nanoparticles as Reporters in Lateral Flow Assays. *Anal. Chem.* **2014**, *86* (19), 9481–9488. https://doi.org/10.1021/ac5012624.

(10) Dodeigne, C.; Thunus, L.; Lejeune, R. Chemiluminescence as Diagnostic Tool. A Review. *Talanta* **2000**, *51* (3), 415–439. https://doi.org/10.1016/s0039-9140(99)00294-5.

(11) Rongen, H. A. H.; Hoetelmans, R. M. W.; Bult, A.; Van Bennekom, W. P. Chemiluminescence and Immunoassays. *J. Pharm. Biomed. Anal.* **1994**, *12* (4), 433–462. https://doi.org/10.1016/0731-7085(94)80027-8.

(12) Kricka, L. Clinical Applications of Chemiluminescence. **2003**. https://doi.org/10.1016/S0003-2670(03)00809-2.

(13) Dyke, K. V. *Luminescence Immunoassay and Molecular Applications*; CRC Press, 1990.

(14) Thorpe, G. H.; Kricka, L. J. Enhanced Chemiluminescent Reactions Catalyzed by Horseradish Peroxidase. *Methods Enzymol.* **1986**, *133*, 331–353. https://doi.org/10.1016/0076-6879(86)33078-7.

(15) Weeks, I.; Beheshti, I.; McCapra, F.; Campbell, A. K.; Woodhead, J. S. Acridinium Esters as High-Specific-Activity Labels in Immunoassay. *Clin. Chem.* **1983**, *29* (8), 1474–1479. https://doi.org/10.1093/clinchem/29.8.1474.

(16) Lumigen. Evaluation of Lumigen HyPerBlu™ Technology for high throughput detection of enzymatically produced hydrogen peroxide http://www.lumigen.com/sites/default/files/additional-documents/hyperblu_research_report.pdf (accessed 2021 -06 -28).

(17) World Health Organization. *Global Report on Diabetes*; World Health Organization: Geneva, Switzerland, 2016.

(18) Todd, J. A. Etiology of Type 1 Diabetes. *Immunity* **2010**, *32* (4), 457–467. https://doi.org/10.1016/j.immuni.2010.04.001.

(19) Bluestone, J. A.; Herold, K.; Eisenbarth, G. Genetics, Pathogenesis and Clinical Interventions in Type 1 Diabetes. *Nature* **2010**, *464* (7293), 1293–1300. https://doi.org/10.1038/nature08933.

(20) Gale, E. a. M. Type 1 Diabetes in the Young: The Harvest of Sorrow Goes On. *Diabetologia* **2005**, *48* (8), 1435–1438. https://doi.org/10.1007/s00125-005-1833-0.

(21) Helminen, O.; Aspholm, S.; Pokka, T.; Hautakangas, M.-R.; Haatanen, N.; Lempainen, J.; Ilonen, J.; Simell, O.; Knip, M.; Veijola, R. HbA(1c) Predicts Time to Diagnosis of Type 1 Diabetes in Children at Risk. *Diabetes* **2015**, *64* (5), 1719–1727. https://doi.org/10.2337/db14-0497.

(22) Atkinson, M. A.; Eisenbarth, G. S.; Michels, A. W. Type 1 Diabetes. *Lancet Lond. Engl.* **2014**, *383* (9911), 69–82. https://doi.org/10.1016/S0140-6736(13)60591-7.

(23) Hirsch, I. B. Clinical Review: Realistic Expectations and Practical Use of Continuous Glucose Monitoring for the Endocrinologist. *J. Clin. Endocrinol. Metab.* **2009**, *94* (7), 2232–2238. https://doi.org/10.1210/jc.2008-2625.

(24) Reinehr, T. Type 2 Diabetes Mellitus in Children and Adolescents. *World J. Diabetes* **2013**, *4* (6), 270–281. https://doi.org/10.4239/wjd.v4.i6.270.

(25) Evert, A. B.; Boucher, J. L.; Cypress, M.; Dunbar, S. A.; Franz, M. J.; Mayer-Davis, E. J.; Neumiller, J. J.; Nwankwo, R.; Verdi, C. L.; Urbanski, P.; Yancy, W.

S. Nutrition Therapy Recommendations for the Management of Adults with Diabetes. *Diabetes Care* **2014**, *37 Suppl 1*, S120-143. https://doi.org/10.2337/dc14-S120.

(26) Bolen, S.; Feldman, L.; Vassy, J.; Wilson, L.; Yeh, H.-C.; Marinopoulos, S.; Wiley, C.; Selvin, E.; Wilson, R.; Bass, E. B.; Brancati, F. L. Systematic Review: Comparative Effectiveness and Safety of Oral Medications for Type 2 Diabetes Mellitus. *Ann. Intern. Med.* **2007**, *147* (6), 386–399. https://doi.org/10.7326/0003-4819-147-6-200709180-00178.

(27) Emerging Risk Factors Collaboration; Sarwar, N.; Gao, P.; Seshasai, S. R. K.; Gobin, R.; Kaptoge, S.; Di Angelantonio, E.; Ingelsson, E.; Lawlor, D. A.; Selvin, E.; Stampfer, M.; Stehouwer, C. D. A.; Lewington, S.; Pennells, L.; Thompson, A.; Sattar, N.; White, I. R.; Ray, K. K.; Danesh, J. Diabetes Mellitus, Fasting Blood Glucose Concentration, and Risk of Vascular Disease: A Collaborative Meta-Analysis of 102 Prospective Studies. *Lancet Lond. Engl.* **2010**, *375* (9733), 2215–2222. https://doi.org/10.1016/S0140-6736(10)60484-9.

(28) Cheung, N.; Mitchell, P.; Wong, T. Y. Diabetic Retinopathy. *Lancet Lond. Engl.* **2010**, *376* (9735), 124–136. https://doi.org/10.1016/S0140-6736(09)62124-3.

(29) Lee, R.; Wong, T. Y.; Sabanayagam, C. Epidemiology of Diabetic Retinopathy, Diabetic Macular Edema and Related Vision Loss. *Eye Vis. Lond. Engl.* **2015**, *2*, 17. https://doi.org/10.1186/s40662-015-0026-2.

(30) Piccoli, G. B.; Grassi, G.; Cabiddu, G.; Nazha, M.; Roggero, S.; Capizzi, I.; De Pascale, A.; Priola, A. M.; Di Vico, C.; Maxia, S.; Loi, V.; Asunis, A. M.; Pani, A.; Veltri, A. Diabetic Kidney Disease: A Syndrome Rather Than a Single Disease.

Rev. Diabet. Stud. RDS **2015**, *12* (1–2), 87–109. https://doi.org/10.1900/RDS.2015.12.87.

(31) Zilliox, L.; Russell, J. W. Treatment of Diabetic Sensory Polyneuropathy. *Curr. Treat. Options Neurol.* **2011**, *13* (2), 143–159. https://doi.org/10.1007/s11940-011-0113-1.

(32) Mathers, C. D.; Loncar, D. Projections of Global Mortality and Burden of Disease from 2002 to 2030. *PLoS Med.* **2006**, *3* (11), e442. https://doi.org/10.1371/journal.pmed.0030442.

(33) NCD Risk Factor Collaboration (NCD-RisC). Worldwide Trends in Diabetes since 1980: A Pooled Analysis of 751 Population-Based Studies with 4.4 Million Participants. *Lancet* **2016**, *387* (10027), 1513–1530. https://doi.org/10.1016/S0140-6736(16)00618-8.

(34) Seuring, T.; Archangelidi, O.; Suhrcke, M. The Economic Costs of Type 2 Diabetes: A Global Systematic Review. *PharmacoEconomics* **2015**, *33* (8), 811–831. https://doi.org/10.1007/s40273-015-0268-9.

(35) Unwin, N.; Marlin, A. WHO and IDF Working Together. *Diabetes Voice* **2004**, *49* (2), 5.

(36) Centers for Disease Control and Prevention. National Diabetes Prevention Program https://www.cdc.gov/diabetes/prevention/index.html (accessed 2021 -06 -28).

(37) American Diabetes Association. Classification and Diagnosis of Diabetes: Standards of Medical Care in Diabetes. *Diabetes Care* **2021**, *44* (Supplement 1), S15–S33.

(38) American Diabetes Association. Diagnosis and Classification of Diabetes Mellitus. *Diabetes Care* **2016**, *36* (Suppl 1), 567–574. https://doi.org/10.2337/dc10-S062.

(39) Peterson, K. P.; Pavlovich, J. G.; Goldstein, D.; Little, R.; England, J.; Peterson, C. M. What Is Hemoglobin A1c? An Analysis of Glycated Hemoglobins by Electrospray Ionization Mass Spectrometry. *Clin. Chem.* **1998**, *44* (9), 1951–1958.

(40) International Expert Committee Report on the Role of the A1C Assay in the Diagnosis of Diabetes. *Diabetes Care* **2009**, *32* (7), 1327–1334. https://doi.org/10.2337/dc09-9033.

(41) *Use of Glycated Haemoglobin (HbA1c) in the Diagnosis of Diabetes Mellitus: Abbreviated Report of a WHO Consultation*; WHO Guidelines Approved by the Guidelines Review Committee; World Health Organization: Geneva, 2011.

(42) Goldstein, D. E.; Little, R. R.; Lorenz, R. A.; Malone, J. I.; Nathan, D.; Peterson, C. M.; Sacks, D. B. Tests of Glycemia in Diabetes. *Diabetes Care* **2004**, *27* (7), 13.

(43) Murata, G. H.; Hoffman, R. M.; Duckworth, W. C.; Wendel, C. S.; Shah, J. H.; Diabetes Outcomes in Veterans Study. Contributions of Weekly Mean Blood Glucose Values to Hemoglobin A1c in Insulin-Treated Type 2 Diabetes: The Diabetes Outcomes in Veterans Study (DOVES). *Am. J. Med. Sci.* **2004**, *327* (6), 319–323. https://doi.org/10.1097/00000441-200406000-00004.

(44) Sacks, D. B.; Arnold, M.; Bakris, G. L.; Bruns, D. E.; Horvath, A. R.; Kirkman, M. S.; Lernmark, A.; Metzger, B. E.; Nathan, D. M. Guidelines and Recommendations for Laboratory Analysis in the Diagnosis and Management of Diabetes Mellitus. *Diabetes Care* **2011**, *34*, 39.

(45) National Diabetes Data Group. Classification and Diagnosis of Diabetes Mellitus and Other Categories of Glucose Intolerance. *Diabetes* **1979**, *28* (12), 1039–1057. https://doi.org/10.2337/diab.28.12.1039.

(46) Report of the Expert Committee on the Diagnosis and Classification of Diabetes Mellitus | Diabetes Care | American Diabetes Association https://diabetesjournals.org/care/article/20/7/1183/22301/Report-of-the-Expert-Committee-on-the-Diagnosis (accessed 2022 -01 -26).

(47) World Health Organization. *Prevention and Control of Noncommunicable Diseases: Guidelines for Primary Health Care in Low Resource Settings*; World Health Organization, 2012.

(48) Global Action Plan for the Prevention and Control of NCDs 2013-2020 https://www.who.int/publications-detail-redirect/9789241506236 (accessed 2022 -01 -26).

(49) Koczula, K. M.; Gallotta, A. Lateral Flow Assays. *Essays Biochem.* **2016**, *60* (1), 111–120. https://doi.org/10.1042/EBC20150012.

(50) Vidarsson, G.; Dekkers, G.; Rispens, T. IgG Subclasses and Allotypes: From Structure to Effector Functions. *Front. Immunol.* **2014**, *5*, 520. https://doi.org/10.3389/fimmu.2014.00520.

(51) Charles A Janeway, J.; Travers, P.; Walport, M.; Shlomchik, M. J. *Immunobiology: The Immune System in Health and Disease*, 5th ed.; Garland Science: New York, NY, 2001.

(52) Swanson, J. A.; Hoppe, A. D. The Coordination of Signaling during Fc Receptor-Mediated Phagocytosis. *J. Leukoc. Biol.* **2004**, *76* (6), 1093–1103. https://doi.org/10.1189/jlb.0804439.

(53) Mégraud, F. Diagnosis of Helicobacter Pylori. *Baillieres Clin. Gastroenterol.* **1995**, *9* (3), 507–518. https://doi.org/10.1016/0950-3528(95)90045-4.

(54) Alexander, T. S. Human Immunodeficiency Virus Diagnostic Testing: 30 Years of Evolution. *Clin. Vaccine Immunol. CVI* **2016**, *23* (4), 249–253. https://doi.org/10.1128/CVI.00053-16.

(55) Jain, A.; Khan, D. N.; Prakash, O.; Shukla, S.; Prakash, S.; Verma, A. K. Severity of Dengue Illness and Presence of Anti DV IgG in Serum of Laboratory Confirmed Dengue Cases. *J. Vector Borne Dis.* **2021**, *58* (3), 228–231. https://doi.org/10.4103/0972-9062.325637.

(56) Kohmer, N.; Westhaus, S.; Rühl, C.; Ciesek, S.; Rabenau, H. F. Clinical Performance of Different SARS-CoV-2 IgG Antibody Tests. *J. Med. Virol.* **2020**, *92* (10), 2243–2247. https://doi.org/10.1002/jmv.26145.

(57) Reuel, N. F.; Grassbaugh, B.; Kruss, S.; Mundy, J. Z.; Opel, C.; Ogunniyi, A. O.; Egodage, K.; Wahl, R.; Helk, B.; Zhang, J.; Kalcioglu, Z. I.; Tvrdy, K.; Bellisario, D. O.; Mu, B.; Blake, S. S.; Van Vliet, K. J.; Love, J. C.; Wittrup, K. D.; Strano, M. S. Emergent Properties of Nanosensor Arrays: Applications for Monitoring IgG Affinity Distributions, Weakly Affined Hypermannosylation, and Colony Selection for Biomanufacturing. *ACS Nano* **2013**, *7* (9), 7472–7482. https://doi.org/10.1021/nn403215e.

(58) Sevilleja, J.; Copeland, C.; Guerrant, R. Detection of a Highly Sensitive Human Fecal Biomarker (10^{-10}) in Less than or Equal to 10 mL Contaminated Drinking Water Using Immunomagnetic Separation. In *American Journal of Tropical Medicine and Hygiene Abstract Book*; 5; 2007; Vol. 77, p 216.

(59) Rodenhuis-Zybert, I. A.; Wilschut, J.; Smit, J. M. Dengue Virus Life Cycle: Viral and Host Factors Modulating Infectivity. *Cell. Mol. Life Sci.* **2010**, *67* (16), 2773–2786. https://doi.org/10.1007/s00018-010-0357-z.

(60) Dengue and severe dengue https://www.who.int/news-room/fact-sheets/detail/dengue-and-severe-dengue (accessed 2022 -03 -03).

(61) CDC - Neglected Tropical Diseases - Diseases https://www.cdc.gov/globalhealth/ntd/diseases/index.html (accessed 2022 -03 -03).

(62) Kularatne, S. A. M. Dengue Fever. *BMJ* **2015**, *351*, h4661. https://doi.org/10.1136/bmj.h4661.

(63) Dwivedi, V. D.; Tripathi, I. P.; Tripathi, R. C.; Bharadwaj, S.; Mishra, S. K. Genomics, Proteomics and Evolution of Dengue Virus. *Brief. Funct. Genomics* **2017**, *16* (4), 217–227. https://doi.org/10.1093/bfgp/elw040.

(64) Mustafa, M. S.; Rasotgi, V.; Jain, S.; Gupta, V. Discovery of Fifth Serotype of Dengue Virus (DENV-5): A New Public Health Dilemma in Dengue Control. *Med. J. Armed Forces India* **2015**, *71* (1), 67–70. https://doi.org/10.1016/j.mjafi.2014.09.011.

(65) Dejnirattisai, W.; Jumnainsong, A.; Onsirisakul, N.; Fitton, P.; Vasanawathana, S.; Limpitikul, W.; Puttikhunt, C.; Edwards, C.; Duangchinda, T.; Supasa, S.; Chawansuntati, K.; Malasit, P.; Mongkolsapaya, J.; Screaton, G. Enhancing Cross-

Reactive Anti-PrM Dominates the Human Antibody Response in Dengue Infection. *Science* **2010**, *328* (5979), 10.1126/science.1185181. https://doi.org/10.1126/science.1185181.

(66) Sridhar, S.; Luedtke, A.; Langevin, E.; Zhu, M.; Bonaparte, M.; Machabert, T.; Savarino, S.; Zambrano, B.; Moureau, A.; Khromava, A.; Moodie, Z.; Westling, T.; Mascareñas, C.; Frago, C.; Cortés, M.; Chansinghakul, D.; Noriega, F.; Bouckenooghe, A.; Chen, J.; Ng, S.-P.; Gilbert, P. B.; Gurunathan, S.; DiazGranados, C. A. Effect of Dengue Serostatus on Dengue Vaccine Safety and Efficacy. *N. Engl. J. Med.* **2018**, *379* (4), 327–340. https://doi.org/10.1056/NEJMoa1800820.

(67) Whitehorn, J.; Farrar, J. Dengue. *Br. Med. Bull.* **2010**, *95* (1), 161–173. https://doi.org/10.1093/bmb/ldq019.

(68) *Dengue Haemorrhagic Fever: Diagnosis, Treatment, Prevention, and Control*, 2nd ed.; World Health Organization, Ed.; World Health Organization: Geneva, 1997.

(69) Raafat, N.; Blacksell, S. D.; Maude, R. J. A Review of Dengue Diagnostics and Implications for Surveillance and Control. *Trans. R. Soc. Trop. Med. Hyg.* **2019**, *113* (11), 653–660. https://doi.org/10.1093/trstmh/trz068.

(70) Hunsperger, E. A.; Muñoz-Jordán, J.; Beltran, M.; Colón, C.; Carrión, J.; Vazquez, J.; Acosta, L. N.; Medina-Izquierdo, J. F.; Horiuchi, K.; Biggerstaff, B. J.; Margolis, H. S. Performance of Dengue Diagnostic Tests in a Single-Specimen Diagnostic Algorithm. *J. Infect. Dis.* **2016**, *214* (6), 836–844. https://doi.org/10.1093/infdis/jiw103.

(71) Chanama, S.; Anantapreecha, S.; A-nuegoonpipat, A.; Sa-gnasang, A.; Kurane, I.; Sawanpanyalert, P. Analysis of Specific IgM Responses in Secondary Dengue Virus Infections: Levels and Positive Rates in Comparison with Primary Infections. *J. Clin. Virol. Off. Publ. Pan Am. Soc. Clin. Virol.* **2004**, *31* (3), 185–189. https://doi.org/10.1016/j.jcv.2004.03.005.

(72) Tang, K. F.; Ooi, E. E. Diagnosis of Dengue: An Update. *Expert Rev. Anti Infect. Ther.* **2012**, *10* (8), 895–907. https://doi.org/10.1586/eri.12.76.

(73) Peeling, R. W.; Artsob, H.; Pelegrino, J. L.; Buchy, P.; Cardosa, M. J.; Devi, S.; Enria, D. A.; Farrar, J.; Gubler, D. J.; Guzman, M. G.; Halstead, S. B.; Hunsperger, E.; Kliks, S.; Margolis, H. S.; Nathanson, C. M.; Nguyen, V. C.; Rizzo, N.; Vázquez, S.; Yoksan, S. Evaluation of Diagnostic Tests: Dengue. *Nat. Rev. Microbiol.* **2010**, *8* (12 Suppl), S30-38. https://doi.org/10.1038/nrmicro2459.

(74) Pal, S.; Dauner, A. L.; Mitra, I.; Forshey, B. M.; Garcia, P.; Morrison, A. C.; Halsey, E. S.; Kochel, T. J.; Wu, S.-J. L. Evaluation of Dengue NS1 Antigen Rapid Tests and ELISA Kits Using Clinical Samples. *PLOS ONE* **2014**, *9* (11), e113411. https://doi.org/10.1371/journal.pone.0113411.

(75) International Diabetes Federation. *IDF Diabetes Atlas, 9th Edition*; Brussels, Belgium, 2019.

(76) Yamanouchi, T.; Tachibana, Y.; Akanuma, H.; Minoda, S.; Shinohara, T.; Moromizato, H.; Miyashita, H.; Akaoka, I. Origin and Disposal of 1,5-Anhydroglucitol, a Major Polyol in the Human Body. *Am. J. Physiol.-Endocrinol. Metab.* **1992**, *263* (2), E268–E273. https://doi.org/10.1152/ajpendo.1992.263.2.E268.

(77) Pitkänen, E. The Serum Polyol Pattern and the Urinary Polyol Excretion in Diabetic and in Uremic Patients. *Clin. Chim. Acta Int. J. Clin. Chem.* **1972**, *38* (1), 221–230. https://doi.org/10.1016/0009-8981(72)90230-6.

(78) Yamanouchi, T.; Akanuma, Y. Serum 1,5-Anhydroglucitol (1,5 AG): New Clinical Marker for Glycemic Control. *Diabetes Res. Clin. Pract.* **1994**, *24* (Suppl 1), S261-268. https://doi.org/10.1016/0168-8227(94)90259-3.

(79) Akanuma, H.; Ogawa, K.; Lee, Y.; Akanuma, Y. Reduced Levels of Plasma 1,5-Anhydroglucitol in Diabetic Patients. *J. Biochem. (Tokyo)* **1981**, *90* (1), 157–162. https://doi.org/10.1093/oxfordjournals.jbchem.a133445.

(80) Yamanouchi, T.; Akanuma, H.; Asano, T.; Konishi, C.; Akaoka, I.; Akanuma, Y. Reduction and Recovery of Plasma 1,5-Anhydro-D-Glucitol Level in Diabetes Mellitus. *Diabetes* **1987**, *36* (6), 709–715. https://doi.org/10.2337/diab.36.6.709.

(81) Yoshioka, S.; Saitoh, S.; Fujisawa, T.; Fujimori, A.; Takatani, O.; Funabashi, M. Identification and Metabolic Implication of 1-Deoxyglucose (1,5-Anhydroglucitol) in Human Plasma. *Clin. Chem.* **1982**, *28* (6), 1283–1286.

(82) Tomen America, Inc. 510(k) Substantial Equivalence Determination Decision Summary, 2003.

(83) Fukumura, Y.; Tajima, S.; Oshitani, S.; Ushijima, Y.; Kobayashi, I.; Hara, F.; Yamamoto, S.; Yabuuchi, M. Fully Enzymatic Method for Determining 1,5-Anhydro-D-Glucitol in Serum. *Clin. Chem.* **1994**, *40* (11 Pt 1), 2013–2016.

(84) Nowatzke, W.; Sarno, M. J.; Birch, N. C.; Stickle, D. F.; Eden, T.; Cole, T. G. Evaluation of an Assay for Serum 1,5-Anhydroglucitol (GlycoMark^{TM}) and

Determination of Reference Intervals on the Hitachi 917 Analyzer. *Clin. Chim. Acta* **2004**, *350* (1), 201–209. https://doi.org/10.1016/j.cccn.2004.08.013.

(85) Yabuuchi, M.; Masuda, M.; Katoh, K.; Nakamura, T.; Akanuma, H. Simple Enzymatic Method for Determining 1,5-Anhydro-D-Glucitol in Plasma for Diagnosis of Diabetes Mellitus. *Clin. Chem.* **1989**, *35* (10), 2039–2043.

(86) Malamud, D.; Rodriguez-Chavez, I. R. Saliva as a Diagnostic Fluid. *Dent. Clin. North Am.* **2011**, *55* (1), 159–178. https://doi.org/10.1016/j.cden.2010.08.004.

(87) Mook-Kanamori, D. O.; Selim, M. M. E.-D.; Takiddin, A. H.; Al-Homsi, H.; Al-Mahmoud, K. A. S.; Al-Obaidli, A.; Zirie, M. A.; Rowe, J.; Yousri, N. A.; Karoly, E. D.; Kocher, T.; Sekkal Gherbi, W.; Chidiac, O. M.; Mook-Kanamori, M. J.; Abdul Kader, S.; Al Muftah, W. A.; McKeon, C.; Suhre, K. 1,5-Anhydroglucitol in Saliva Is a Noninvasive Marker of Short-Term Glycemic Control. *J. Clin. Endocrinol. Metab.* **2014**, *99* (3), E479-483. https://doi.org/10.1210/jc.2013-3596.

(88) Halama, A.; Kulinski, M.; Kader, S. A.; Satheesh, N. J.; Abou-Samra, A. B.; Suhre, K.; Mohammad, R. M. Measurement of 1,5-Anhydroglucitol in Blood and Saliva: From Non-Targeted Metabolomics to Biochemical Assay. *J. Transl. Med.* **2016**, *14* (1), 140. https://doi.org/10.1186/s12967-016-0897-6.

(89) Topkas, E.; Keith, P.; Dimeski, G.; Cooper-White, J.; Punyadeera, C. Evaluation of Saliva Collection Devices for the Analysis of Proteins. *Clin. Chim. Acta* **2012**, *413* (13–14), 1066–1070. https://doi.org/10.1016/j.cca.2012.02.020.

(90) Holm-Hansen, C.; Tong, G.; Davis, C.; Abrams, W. R.; Malamud, D. Comparison of Oral Fluid Collectors for Use in a Rapid Point-of-Care Diagnostic Device. *Clin.*

Diagn. Lab. Immunol. **2004**, *11* (5), 909–912. https://doi.org/10.1128/CDLI.11.5.909-912.2004.

(91) Navazesh, M. Methods for Collecting Saliva. *Ann. N. Y. Acad. Sci.* **1993**, *694*, 72–77. https://doi.org/10.1111/j.1749-6632.1993.tb18343.x.

(92) Bhatt, S.; Gething, P. W.; Brady, O. J.; Messina, J. P.; Farlow, A. W.; Moyes, C. L.; Drake, J. M.; Brownstein, J. S.; Hoen, A. G.; Sankoh, O.; Myers, M. F.; George, D. B.; Jaenisch, T.; Wint, G. R. W.; Simmons, C. P.; Scott, T. W.; Farrar, J. J.; Hay, S. I. The Global Distribution and Burden of Dengue. *Nature* **2013**, *496* (7446), 504–507. https://doi.org/10.1038/nature12060.

(93) Guzman, M. G.; Vazquez, S. The Complexity of Antibody-Dependent Enhancement of Dengue Virus Infection. *Viruses* **2010**, *2* (12), 2649–2662. https://doi.org/10.3390/v2122649.

(94) GBD 2017 Causes of Death Collaborators. Global, Regional, and National Age-Sex-Specific Mortality for 282 Causes of Death in 195 Countries and Territories, 1980-2017: A Systematic Analysis for the Global Burden of Disease Study 2017. *Lancet Lond. Engl.* **2018**, *392* (10159), 1736–1788. https://doi.org/10.1016/S0140-6736(18)32203-7.

(95) Ayukekbong, J. A.; Oyero, O. G.; Nnukwu, S. E.; Mesumbe, H. N.; Fobisong, C. N. Value of Routine Dengue Diagnosis in Endemic Countries. *World J. Virol.* **2017**, *6* (1), 9–16. https://doi.org/10.5501/wjv.v6.i1.9.

(96) Thomas, L.; Najioullah, F.; Verlaeten, O.; Martial, J.; Brichler, S.; Kaidomar, S.; Moravie, V.; Cabié, A.; Césaire, R. Relationship between Nonstructural Protein 1

Detection and Plasma Virus Load in Dengue Patients. *Am. J. Trop. Med. Hyg.* **2010**, *83* (3), 696–699. https://doi.org/10.4269/ajtmh.2010.10-0138.

(97) Hunsperger, E. A.; Yoksan, S.; Buchy, P.; Nguyen, V. C.; Sekaran, S. D.; Enria, D. A.; Vazquez, S.; Cartozian, E.; Pelegrino, J. L.; Artsob, H.; Guzman, M. G.; Olliaro, P.; Zwang, J.; Guillerm, M.; Kliks, S.; Halstead, S.; Peeling, R. W.; Margolis, H. S. Evaluation of Commercially Available Diagnostic Tests for the Detection of Dengue Virus NS1 Antigen and Anti-Dengue Virus IgM Antibody. *PLoS Negl. Trop. Dis.* **2014**, *8* (10), e3171. https://doi.org/10.1371/journal.pntd.0003171.

(98) Hunsperger, E. A.; Sharp, T. M.; Lalita, P.; Tikomaidraubuta, K.; Cardoso, Y. R.; Naivalu, T.; Khan, A. S.; Marfel, M.; Hancock, W. T.; Tomashek, K. M.; Margolis, H. S. Use of a Rapid Test for Diagnosis of Dengue during Suspected Dengue Outbreaks in Resource-Limited Regions. *J. Clin. Microbiol.* **2016**, *54* (8), 2090–2095. https://doi.org/10.1128/JCM.00521-16.

(99) Gelanew, T.; Poole-Smith, B. K.; Hunsperger, E. Development and Characterization of Mouse Monoclonal Antibodies against Monomeric Dengue Virus Non-Structural Glycoprotein 1 (NS1). *J. Virol. Methods* **2015**, *222*, 214–223. https://doi.org/10.1016/j.jviromet.2015.06.003.

(100) Dawes, C. Effects of Diet on Salivary Secretion and Composition. *J. Dent. Res.* **1970**, *49* (6), 1263–1273. https://doi.org/10.1177/00220345700490061501.

(101) Gonzalez-Moa, M. J.; Van Dorst, B.; Lagatie, O.; Verheyen, A.; Stuyver, L.; Biamonte, M. A. Proof-of-Concept Rapid Diagnostic Test for Onchocerciasis: Exploring Peptide Biomarkers and the Use of Gold Nanoshells as Reporter

Nanoparticles. *ACS Infect. Dis.* **2018**, *4* (6), 912–917. https://doi.org/10.1021/acsinfecdis.8b00031.

(102) Scholz, F.; Rüttinger, L.; Heckmann, T.; Freund, L.; Gad, A.-M.; Fischer, T.; Gütter, A.; Söffing, H. H. Carboxyl Functionalized Gold Nanorods for Sensitive Visual Detection of Biomolecules. *Biosens. Bioelectron.* **2020**, *164*, 112324. https://doi.org/10.1016/j.bios.2020.112324.

(103) Battino, M.; Ferreiro, M. S.; Gallardo, I.; Newman, H. N.; Bullon, P. The Antioxidant Capacity of Saliva. *J. Clin. Periodontol.* **2002**, *29* (3), 189–194. https://doi.org/10.1034/j.1600-051x.2002.290301x.x.

(104) Saleh, L.; Plieth, C. Total Low-Molecular-Weight Antioxidants as a Summary Parameter, Quantified in Biological Samples by a Chemiluminescence Inhibition Assay. *Nat. Protoc.* **2010**, *5* (10), 1627–1634. https://doi.org/10.1038/nprot.2010.120.

(105) Moore, S.; Calder, K. A.; Miller, N. J.; Rice-Evans, C. A. Antioxidant Activity of Saliva and Periodontal Disease. *Free Radic. Res.* **1994**, *21* (6), 417–425. https://doi.org/10.3109/10715769409056594.

(106) Mäkilä, E.; Kirveskari, P. A Study of Ascorbic Acid in Human Saliva. *Arch. Oral Biol.* **1969**, *14* (11), 1285–1292. https://doi.org/10.1016/0003-9969(69)90201-5.

(107) Soini, H. A.; Klouckova, I.; Wiesler, D.; Oberzaucher, E.; Grammer, K.; Dixon, S. J.; Xu, Y.; Brereton, R. G.; Penn, D. J.; Novotny, M. V. Analysis of Volatile Organic Compounds in Human Saliva by a Static Sorptive Extraction Method and Gas Chromatography-Mass Spectrometry. *J. Chem. Ecol.* **2010**, *36* (9), 1035–1042. https://doi.org/10.1007/s10886-010-9846-7.

(108) de Almeida, P. D. V.; Grégio, A. M. T.; Machado, M. A. N.; de Lima, A. A. S.; Azevedo, L. R. Saliva Composition and Functions: A Comprehensive Review. *J. Contemp. Dent. Pract.* **2008**, *9* (3), 72–80.

APPENDICES

A.1. Quantification of 1,5-anhydroglucitol in saliva

A.1.1. Materials

Glucose oxidase at 168.1 kU/g (all unit definitions herein are 1 μmol of product produced per minute) from Aspergillus niger, galactose oxidase at 1500 U/mg from *Dactylium dendroides*, pyranose oxidase at 10.4 U/mg from *Coriolus sp.*, uricase at 4.5 U/mg from *Candida sp.*, catalase at 4998 U/mg from bovine liver, and horseradish peroxidase (HRP) at 250 U/mg were purchased from Sigma-Aldrich (St. Louis, MO). 1,5-Anhydroglucitol (AHG) 50 μg/mL calibration standard was purchased from GlycoMark (New York, NY). FemtoGlow luminol was purchased from Michigan Diagnostics (Royal Oak, MI). HyPerBlu chemiluminescent reagent was purchased from Lumigen (Southfield, MI). Sarstedt Salivette® cotton swabs were purchased from Thermo Fisher Scientific (Hampton, NH). Amicon Ultra 0.5 mL 3 kDa centrifugal filters were purchased from EMD Millipore (Burlington, MA).

A.1.2. Initial attempts to measure AHG in saliva by luminol chemiluminescence

A.1.2.1. Methods

Thawed saliva (50 μL) was first pre-treated with 5 μL each of uricase (50 U/mL in PBS, pH 7.4) and catalase (50 U/mL in PBS, pH 7.4). After a 30-minute incubation at 37°C, the saliva was transferred to an Amicon ultra 3 kDa centrifugal filter and centrifuged at 14,000 g for 30 min to remove the enzymes. The treated saliva was then injected into a custom-made portable luminometer. The luminometer consists of a microPMT (Hamamatsu Photonics; cat. H12406), microcontroller, 3D printed housing, and injection tubing allowing real-time signal acquisition during sequential enzyme

injections. Following the injection of the saliva, 50 μL of FemtoGlow chemiluminescent substrate (Michigan Diagnostics; Royal Oak, MI) and 5 μL of HRP (10 ng/mL in PBS, pH 7.4) were injected into the luminometer. Finally, 5 μL glucose oxidase (20 U/mL in PBS, pH 7.4), galactose oxidase (20 U/mL in PBS, pH 7.4), and pyranose oxidase (2.7 U/mL in PBS, pH 7.4) were sequentially injected into the sample, and changes in luminescence observed.

A.1.2.2. Results

Because salivary AHG levels are lower than in blood, we selected a chemiluminescence approach to detecting hydrogen peroxide produced by pyranose oxidase oxidation of AHG. Initial attempts to measure AHG in saliva with luminol-based chemiluminescence were unsuccessful due to the strong inhibition of light production by compounds present in saliva. As shown in Fig. A.1, after enzymatically clearing glucose and galactose from serum and saliva samples (with glucose oxidase and galactose oxidase, respectively, followed by catalase and ultrafiltration), pyranose oxidase, luminol (FemtoGlow), and HRP were added to the samples. The saliva sample did not show any signal even when spiked with 180 mM of hydrogen peroxide, suggesting that some component(s) of saliva inhibit luminol chemiluminescence.

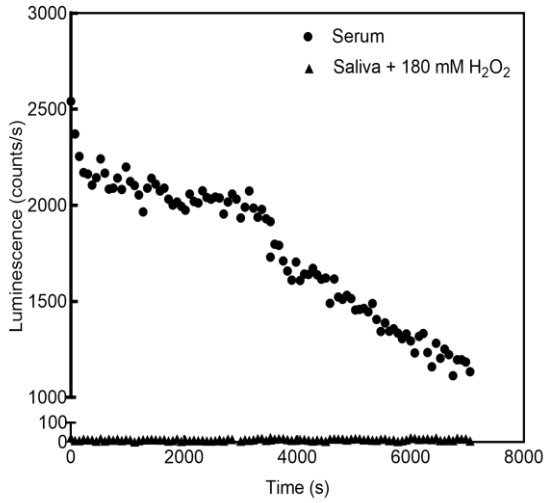

Figure A.1. Luminescent intensity following clearance with glucose oxidase, galactose oxidase, and ultrafiltration of saliva spiked with 180 mM hydrogen peroxide and serum treated with pyranose oxidase, FemtoGlow, and HRP.

Saliva is known to have a high concentration of antioxidants, and a luminol-based chemiluminescence inhibition assay is used to quantify total antioxidative capacity[103,104]. For example, uric acid present in saliva is a potent antioxidant that scavenges singlet oxygen and radicals[105]. Other antioxidants (e.g., ascorbic acid and uric acid) and antioxidant enzymes (e.g., catalase and superoxide dismutase) also are present in lesser amounts[106]. Removal of uric acid with uricase increased the production of luminescence by the luminol-peroxide reaction (Fig. A.2) compared to the untreated saliva sample. Filtration or uricase treatment alone showed modest improvement, suggesting that the inhibition is the cumulative effect of antioxidants, possibly other small metabolites, larger peptides, and enzymes (Fig. A.2). After uricase treatment and filtration, we could detect AHG in saliva through subsequent depletion of interfering glucose and galactose (Fig. A.3).

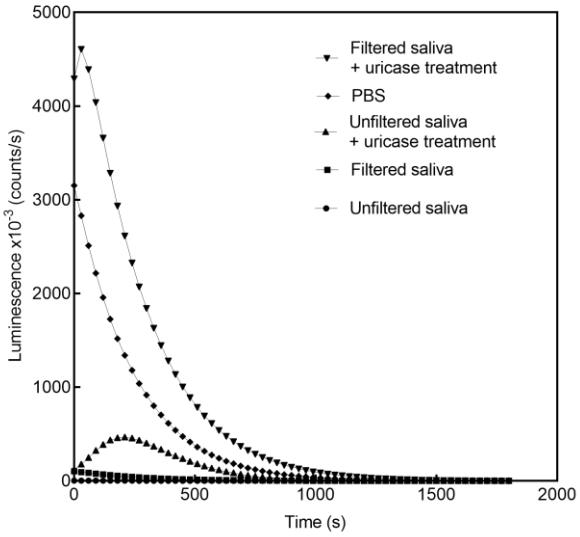

Figure A.2. Luminol (FemtoGlow)-HRP chemiluminescence of saliva or buffer spiked with 100 µM H_2O_2 after various treatments. Untreated saliva (circles, bottom) showed no detectable signal.

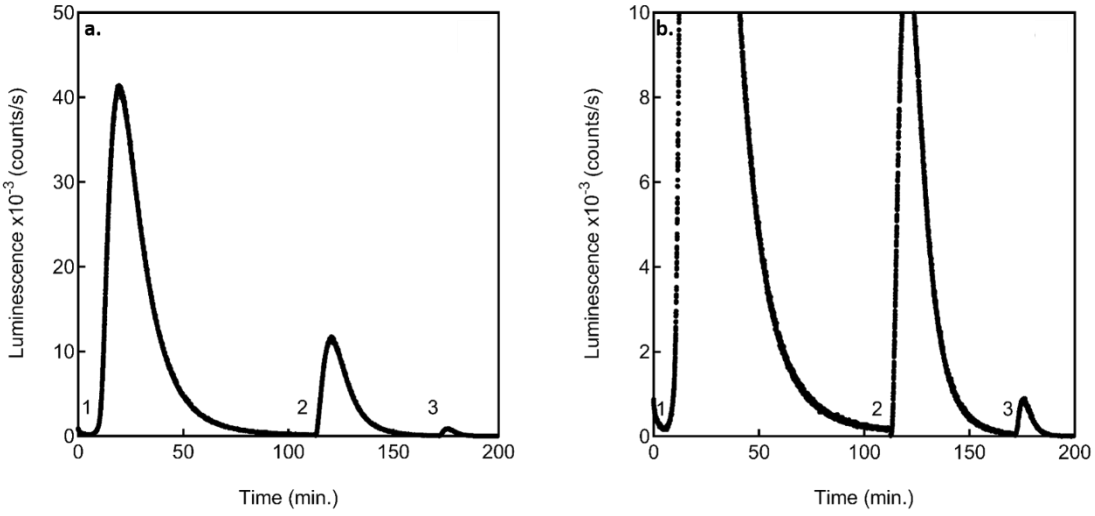

Figure A.3. (a) Detection of hydrogen peroxide produced from (1) glucose, (2) galactose, and (3) AHG in saliva. (b) After treating saliva with uricase, catalase, and ultrafiltration, (1) glucose oxidase was injected, (2) then galactose oxidase, (3) and pyranose oxidase.

The chemiluminescent reagent used to detect hydrogen peroxide ideally would be unaffected by quenching compounds. Lumigen HyPerBlu™ is a dioxetane-boronic acid that reacts directly with hydrogen peroxide to produce a sustained chemiluminescent signal. This characteristic allows HyPerBlu to resist many forms of quenching[16]. Unlike luminol, HyPerBlu is a one-step reagent that does not require HRP or other cofactors and produces sustained and robust luminescence rather than a short flash of light, making it easier to measure at point-of-care and further motivating the choice of HyPerBlu to quantify AHG in saliva.

A.1.3. Evaluation of saliva AHG concentration by LC-MS

A.1.3.1. Methods

Saliva analysis by liquid chromatography-mass spectrometry (LC-MS) was performed at the Proteomics and Metabolomics Facility of The University of Texas M.D. Anderson Cancer Center (Houston, TX). Specimens were first thawed on ice, then centrifuged at 17,000 g for five minutes at 4°C to precipitate any mucus or particulates. Saliva aliquots of 500 μL were treated with 2 mL of 0.1% formic acid in a 90/10 mixture of acetonitrile and water and vortexed for two minutes, then centrifuged a second time at 17,000 g for five minutes at 4°C. After centrifuging, the resulting supernatant was transferred to clean containers, evaporated, reconstituted in 100 μL of deionized water, vortexed, and centrifuged a final time at 17,000 g for five minutes at 4°C. The supernatant from the samples was then transferred into auto-sampler vials for LC-MS analysis. The analysis was performed using an ICS5000+ system coupled with a Thermo Fusion OrbiTrap ESI operated in positive mode. The sample flow rate was 0.3 mL/min through a Dionex IonPac AS11 2x250 mm liquid chromatography column at 30°C. The

make-up solvent was a 1 mM lithium chloride in methanol flowing at 0.05 mL/min. Total time detection was 10 minutes with a 10 – 90 mM potassium hydroxide gradient.

A.1.3.2. Results

LC-MS was used for orthogonal confirmation (beyond the calibrations described above) of the accuracy of the assay. Saliva is primarily composed of water and contains many other minor components, including mucus, digestive enzymes, growth factors, cytokines, immunoglobulins, antibacterial peptides, bacterial cells, salts, and low molecular weight metabolites[107,108]. Two control saliva samples from a single individual (IRB ID CR00000501) were analyzed by LC-MS at the Proteomics and Metabolomics Facility at The University of Texas M.D. Anderson Cancer Center to determine the concentration of AHG in the saliva.

The chromatogram and spectrum obtained from the analysis of one of the two saliva samples are shown in Fig. A.4. We established a calibration curve by analyzing several solutions of known AHG concentration and correlating the solutions with their resultant liquid chromatography peak areas (Fig. A.5). From the linear fit of the curve, we determined that the total concentrations of AHG found in the two saliva samples were 0.62 and 0.66 μg/mL, averaging 0.64 μg/mL. From this same sample, we determined the salivary AHG concentration by our method to be approximately 0.76 ± 0.14 μg/mL from three replicates, a difference of 18.8%, independently confirming the accuracy of the chemiluminescent assay.

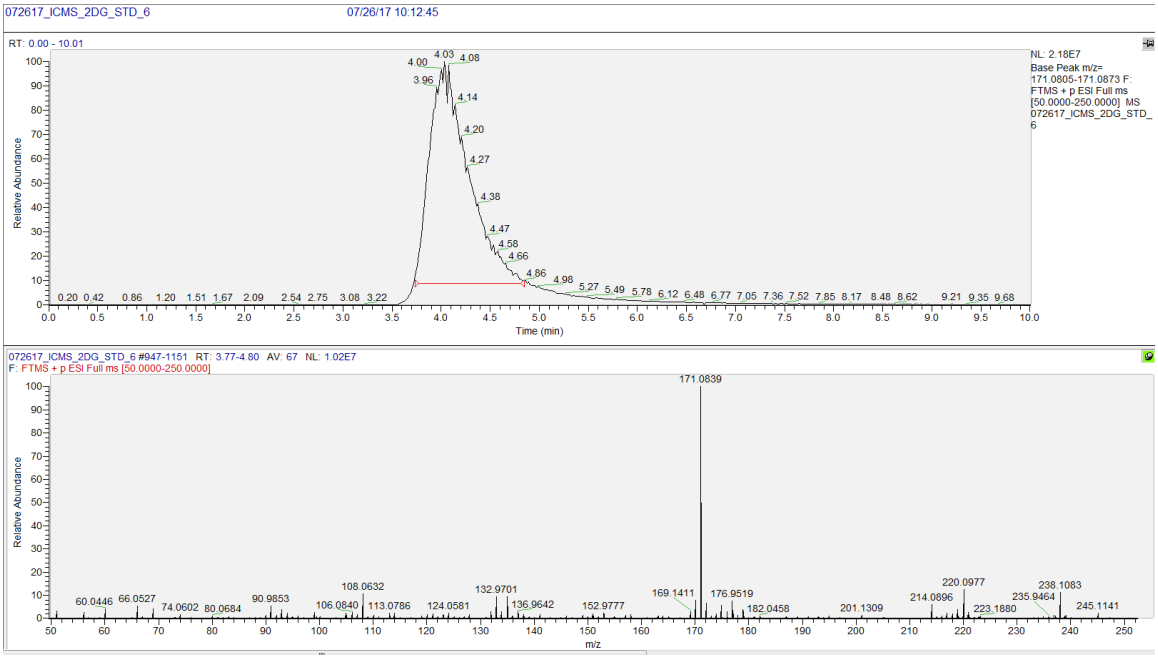

Figure A.4. Chromatogram and spectrum obtained from analysis of saliva by LC-MS.

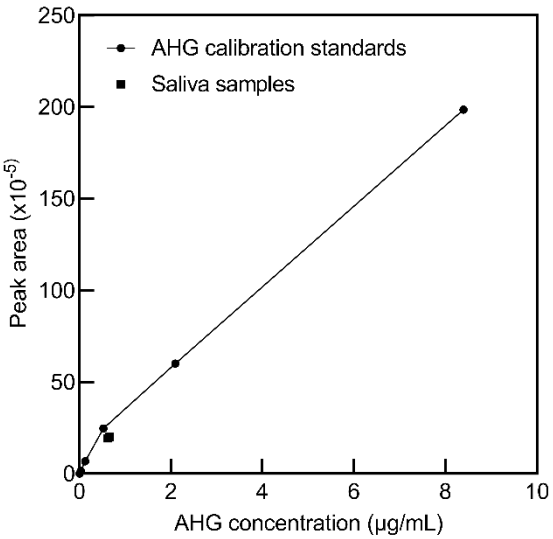

Figure A.5. Calibration curve used to quantify 1,5-anhydroglucitol concentration in saliva by LC-MS.

A.2. Comparison of rapid human IgG detection by colorimetric and nanophosphor lateral flow assays

A.2.1. Additional lateral flow replicates

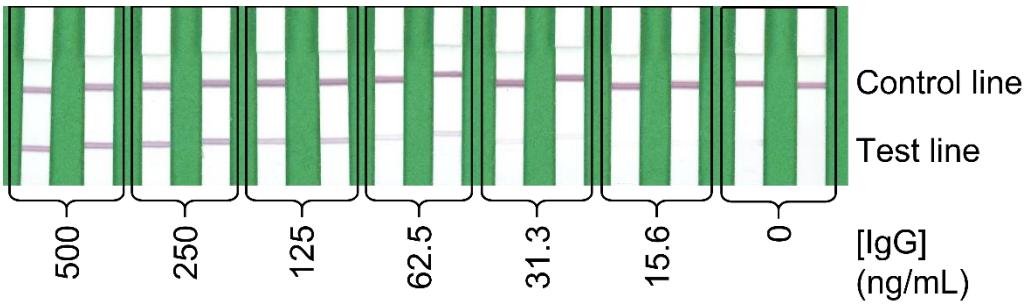

Figure A.6. Detection of human IgG by colloidal gold nanoparticle lateral flow assay replicates.

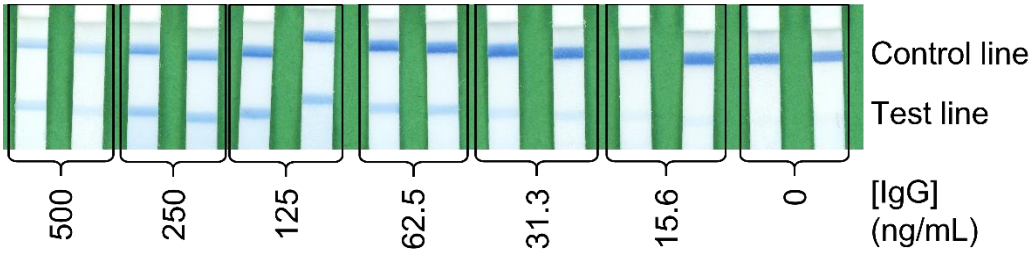

Figure A.7. Detection of human IgG by blue latex nanoparticle lateral flow assay replicates.

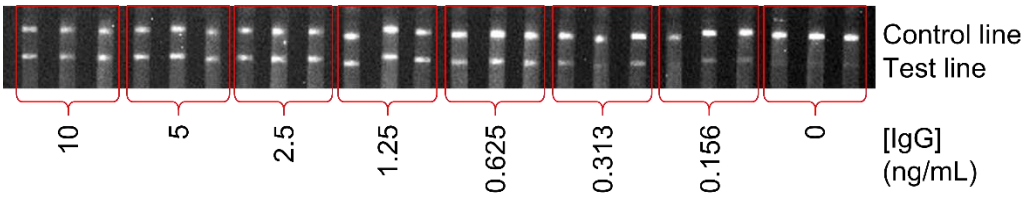

Figure A.8. Detection of human IgG by nanophosphor lateral flow assay replicates.

A.3. Sensitive detection of dengue NS1 by nanophosphor lateral flow immunoassay

A.3.1. Additional lateral flow replicates

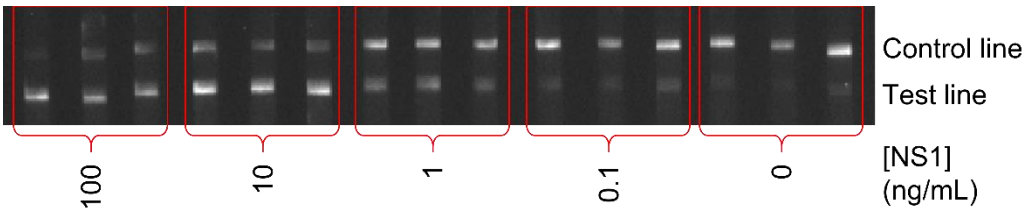

Figure A.9. Detection of dengue virus non-structural protein 1 by nanophosphor lateral flow assay replicates imaged by FluorChem.

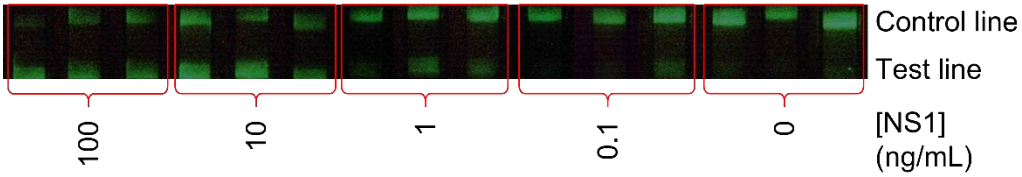

Figure A.10. Detection of dengue virus non-structural protein 1 by nanophosphor lateral flow assay replicates imaged by iPhone 5s.